A small deformations effective stress model of gradient plasticity phase-field fracture

Alessandro Marengo[a,*], Umberto Perego[a]

[a]Department of Civil and Environmental Engineering, Politecnico di Milano, P.zza L. da Vinci 32, 20133 Milan, Italy

Abstract

A variational formulation of small strain ductile fracture, based on a phase-field modeling of crack propagation, is proposed. The formulation is based on an effective stress description of gradient plasticity, combined with an AT1 phase-field model. Starting from established variational statements of finite-step elastoplasticity for generalized standard materials, a mixed variational statement is consistently derived, incorporating in a rigorous way a variational finite-step update for both the elastoplastic and the phase-field dissipations. The complex interaction between ductile and brittle dissipation mechanisms is modeled by assuming a plasticity driven crack propagation model. A non-variational function of the equivalent plastic strain is then introduced to modulate the phase-field dissipation based on the developed plastic strains. Particular care has been devoted to the formulation of a consistent Newton-Raphson scheme for the case of Mises plasticity, with a global return mapping and relative tangent matrix, supplemented by a line-search scheme, for the solution of the gradient elastoplasticity problem for fixed phase field. The resulting algorithm has proved to be very robust and computationally effective. Application to several benchmark tests show the robustness and accuracy of the proposed model.

Keywords: Phase field, Gradient plasticity, Ductile fracture, Linear complementarity problem, Staggered scheme, Finite element analysis

1. Introduction

Fracture propagation in elastoplastic solids presents a ductile dissipation mechanism, due to the development of plastic strains, competing and interacting with a brittle dissipation mechanism, due to the generation of new fracture surfaces. The existence of a large scale plastic zone makes Griffith approach to

*Corresponding author

Email addresses: alessandro.marengo@polimi.it (Alessandro Marengo), umberto.perego@polimi.it (Umberto Perego)

brittle fracture inapplicable, as much as its elegant and well-established phase-field variational formulation introduced in [1, 2]. Several authors have proposed extensions of the phase-field formulation of brittle fracture incorporating plastic dissipation mechanisms. In the small deformation framework, local plasticity has been addressed, e.g., in [3, 4, 5, 4, 6, 7, 8, 9], while gradient plasticity mechanisms have been considered in [10, 11, 12, 13]. In the large deformation framework, the models [14, 15, 16, 17, 18] deal with local plasticity, while gradient plasticity has been included in the formulation in [19, 20, 21]. A comparative review of some small-strain ductile fracture models can be found in [22].

In the present work, a variational formulation of small strain ductile fracture, based on a phase-field modeling of crack propagation, is proposed. Starting from established variational statements of finite-step elastoplasticity for generalized standard materials [23, 24, 25, 26, 27, 28, 29], a rather general mixed variational statement, applicable to a wide class of elastoplastic materials, is consistently derived, incorporating in a rigorous way a variational finite-step update for both the elastoplastic and the phase-field dissipations.

The formulation is based on an effective stress [10, 19, 6, 7, 13] description of gradient plasticity, combined with an AT1 phase-field model [30, 31, 17, 16, 13]. The term *effective stress* refers here to the true stress acting on the undamaged portion of the bulk material. The value of the effective stress is then not affected by developing damage. The main consequence of this choice is that plasticity continues to develop until the very final state of material failure, where damage approaches unity. This is in contrast to what happens when plasticity is described in terms of nominal stresses, i.e., when stress are reduced by the current value of damage while the yield stress remains unchanged. In this latter case, as soon as damage starts to develop, the nominal stress decreases and the yield condition is no more satisfied, so that the final part of material deformation is purely brittle (for a discussion on effective vs nominal stresses see, e.g., [6]). It should be noted that other models, where the yield stress is degraded by damage in a way different from the one used for stresses and, therefore, not fitting into the nominal and effective stress classification proposed here, have been presented in the literature (see, e.g., [3, 22, 10]). Unlike for the nominal stress case, for these models it is possible that damage and plasticity evolve together.

The fact that effective stresses are used and that plasticity continues to grow also in the damage localization phase, implies that, after damage has started to develop and the global structural response has become softening, incremental plastic strains tend to localize in a one-element-thick band, giving rise to a pathological mesh dependence in the final stage of rupture [21]. To avoid the problem, the simple and effective gradient plasticity regularization proposed in [32] is here adopted. The presence of the gradient plasticity term introduces computational difficulties for the finite-step time integration of the nonlocal constituive law. A computationally effective and robust Newton-Raphson scheme for the solution of the gradient elastoplastic problem for fixed damage is therefore proposed for the case of Mises plasticity, together with its global return mapping algorithm and expression of the global consistent tangent matrix. This global return mapping scheme allows to formulate the finite-step elastoplastic problem as a global linear complementarity problem. The same has been done for the phase-field problem, so that irreversibility of both plastic and brittle dissipation turns out to be enforced in a rigorous way. Both linear complementarity problems have been solved using a very efficient explicit Projected Successive Over-Relaxation (PSOR) algorithm [33], following the approach proposed in [32, 34].

In ductile fracture, either already existing voids, or voids nucleated under the effect of developing plastic strains at inclusions or second-phase particles, grow until they coalesce giving rise to a continuous fracture path. Voids nucleation and growth is associated to locally high levels of plastic deformation, suggesting that in most cases ductile fracture requires high levels of energy absorption (see, e.g., [35]). Based on these physical observations, in the proposed phase-field plasticity model, crack nucleation and propagation is assumed to be driven by plasticity. Damage development is then possible when the plastic process zone in a stress concentration region reaches a critical level, measured by the equivalent plastic strain. In practical terms, this is achieved in the model by introducing in the damage activation condition a non-variational function of the equivalent plastic strain, modulating the effective value of the material fracture energy. This is somehow in line with what has been done by several other authors ([7, 9, 17]), though making use of a substantially different definition of the fracture energy modulation function. Another important aspect, clearly emerging from the considered numerical applications, is the capability of the proposed plasticity driven approach to predict crack nucleation in the absence of a pre-existing crack (for a discussion on phase-field prediction of crack nucleation see, e.g., [36, 37]).

The AT1 model used here has some key conceptual and practical advantages over the AT2 model: it has a non-zero elastic limit, preventing diffuse damage at small loading and the damage localization band is of finite width [36]. Both features are of importance in the considered plasticity driven framework: i) the material response remains linear elastic until the yield limit is achieved, without any damage development; ii) having a finite width, it is possible to define the phase-field characteristic length so that the phase-field localization band remains entirely contained within the plasticity process zone.

The paper is organized as follows. In Section 2 the phase-field model to ductile fracture is built starting from a consistent thermodynamic formulation in rate form. Then, the discrete finite-step governing equations and evolution laws are derived with a Hu-Washizu variational approach. Finally, the main constitutive choices are presented. In Section 3 the fracture activation criterion is modified with the introduction of a non-variational modulation function f. Its optimal profile is derived based on a 1D homogeneus model and the meaning of the additional material parameters is discussed. In Section 4 the spatial discretization of the governing equations is performed. In Section 5 algorithmic aspects, such as the alternate minimization scheme and the elastoplastic monolithic scheme, are detailed. In Section 6 numerical applications to several benchmark problems are presented and discussed.

2. Phase-field ductile fracture

2.1. Nominal & effective responses

Let $\Omega_0 \subset \mathbb{R}^{n_{dim}}$ be the reference domain, where n_{dim} is the problem dimension. It is subject to Dirichelet boundary conditions on $\partial\Omega_D$ and Neumann boundary conditions on $\partial\Omega_N$ with $\partial\Omega_D \cup \partial\Omega_N = \partial\Omega_0$ and $\partial\Omega_D \cap \partial\Omega_N = \emptyset$. The displacement field $\mathbf{u}$ is subject to $\mathbf{u} = \mathbf{u}_D$ on $\partial\Omega_D$. The phase-field damage-like variable d is a scalar quantity ranging from 0 to 1 interpolating the unbroken and fully broken state of the material, respectively. The material degradation function $\omega(d)$, also often referred to as *continuity function*, accounts for the presence of damage in the material bulk and it is such that $\omega(0) = 1$, $\omega(1) = 0$ and $\omega'(d) < 0$. In the damaged state, $d\Omega_0$ defines the infinitesimal nominal volume, equal to the original undamaged volume, while $d\Omega = \omega \; d\Omega_0$ is the current effective volume, i.e., the nominal volume minus the volume of the defects. A sketch of the different volumes is shown in Figure 1, where Ω_V is the micro-voids volume. Note that, while Ω_0 denotes the nominal volume and Ω the effective one, in what follows the effective quantities, i.e., quantities referred to the damaged volume, are always denoted with a zero subscript $(\cdot)_0$, while the nominal quantities, i.e., those referred to the undamaged volume, do not have a zero subscript. The pointwise transformation from effective to nominal quantity reads:

$$\underbrace{(\cdot)_0}_{effective} \; \underbrace{d\Omega}_{effective} = \underbrace{(\cdot)_0}_{effective} \; \omega \; \underbrace{d\Omega_0}_{nominal} = \underbrace{(\cdot)}_{nominal} \; \underbrace{d\Omega_0}_{nominal} \tag{1}$$

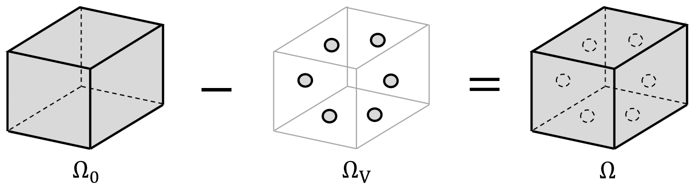

Figure 1: Nominal Ω_0, voids Ω_V, and effective Ω volumes

2.2. *State variables & evolution laws*

An elastoplastic material, belonging to the class of *generalized standard materials* [38], is considered. The material state is assumed to be completely defined by the total strain tensor $\boldsymbol{\varepsilon} := \boldsymbol{\nabla}^s \mathbf{u}$ ($\boldsymbol{\nabla}^s(\cdot)$ being the symmetric gradient operator), the plastic strain tensor $\boldsymbol{\varepsilon}^p$, the hardening internal variable α, and the damage-like phase field d. The free energy ψ density is assumed to be additively decomposed into its elastic (reversible) part $\omega\,\psi_0^e(\boldsymbol{\varepsilon}^e)$, $\boldsymbol{\varepsilon}^e = \boldsymbol{\varepsilon} - \boldsymbol{\varepsilon}^p$ denoting the elastic strain tensor, and hardening (unrecoverable) $\omega\,\psi_0^p(\alpha)$ part, the latter being the internal elastic energy stored in the material because of irreversible deformations of the microstructure. The energies $\psi_0^e(\boldsymbol{\varepsilon}^e)$ and $\psi_0^p(\alpha)$, assumed to be convex functions of their arguments, are the undamaged or *effective* elastic and hardening free energies. The *nominal* and *effective* free energy densities are defined as:

$$\psi := \omega\,\psi_0 \quad , \quad \psi_0 := \psi_0^e + \psi_0^p \tag{2}$$

The Clausius-Duhem inequality states that the specific dissipation rate $\dot{\phi}$ must increase in every transformation, i.e. $\dot{\phi} := \boldsymbol{\sigma} : \dot{\boldsymbol{\varepsilon}} - \dot{\psi} \geq 0$, where $\boldsymbol{\sigma}$ is the Cauchy stress tensor, $\dot{\boldsymbol{\varepsilon}}$ is the total strain rate, and $\dot{\psi}$ is the free energy rate. The introduction of (2) into the dissipation inequality reads:

$$\dot{\phi} := \boldsymbol{\sigma} : \dot{\boldsymbol{\varepsilon}} - \dot{\psi} = \underbrace{(\boldsymbol{\sigma} - \omega\,\partial_{\boldsymbol{\varepsilon}^e}\psi_0^e) : \dot{\boldsymbol{\varepsilon}}^e}_{elastic} + \underbrace{\boldsymbol{\sigma} : \dot{\boldsymbol{\varepsilon}}^p - \omega\,\partial_\alpha \psi_0^p\;\dot{\alpha}}_{plastic} - \underbrace{\omega'\;\psi_0\;\dot{d}}_{fracture} \geq 0 \tag{3}$$

During an elastic or reversible transformation, no evolution of the plastic deformations $\dot{\boldsymbol{\varepsilon}}^p = \mathbf{0}$, of the hardening variable $\dot{\alpha} = 0$ or of damage $\dot{d} = 0$ occurs and, hence, no dissipation increase is produced (i.e., $\dot{\phi} = 0$). Therefore, the only term left is $(\boldsymbol{\sigma} - \omega\,\partial_{\boldsymbol{\varepsilon}}\psi_0^e) : \dot{\boldsymbol{\varepsilon}} = 0$. Since it must hold for all reversible transformations $\dot{\boldsymbol{\varepsilon}}$, the nominal and effective elastic evolution laws read:

$$\boldsymbol{\sigma} = \omega\,\boldsymbol{\sigma}_0 \quad , \quad \boldsymbol{\sigma}_0 := \partial_{\boldsymbol{\varepsilon}^e}\psi_0^e \tag{4}$$

Consideration of the dissipation inequality in the conditions of no damage, $\dot{d} = 0$, allows to define:

$$\dot{\phi}^p = \omega\,\dot{\phi}_0^p \quad , \quad \dot{\phi}_0^p := \boldsymbol{\sigma}_0 : \dot{\boldsymbol{\varepsilon}}^p - \chi_0 \cdot \dot{\alpha} \geq 0 \tag{5}$$

where $\dot{\phi}_0^p$ denotes the dissipation rate due to plasticity only and χ_0 is the effective *static* hardening variable, i.e. the thermodynamic force work-conjugated to the internal variable α. From (3), it turns out to be defined as:

$$\chi_0 := \partial_\alpha \psi_0^p \tag{6}$$

The elastoplastic dissipation inequality $(5)_2$ can be also expressed in terms of its effective counterpart, i.e., $\dot{\phi}^p d\Omega_0 = \dot{\phi}_0^p d\Omega \geq 0$. The effective yield stress associated to the internal variable α is $\sigma_{y0}(\alpha) = \bar{\sigma}_{y0} + \chi_0(\alpha)$, where $\bar{\sigma}_{y0}$ is the initial yield stress. The elastoplastic evolution has to satisfy the additional constraint that the admissible set of effective stress and hardening parameter $(\boldsymbol{\sigma}_0^*, \chi_0^*)$ has to fullfil the yield criterion $f_y(\boldsymbol{\sigma}_0^*, \chi_0^*) \leq 0$, where f_y is the local yield function, convex in the space of stress and static internal variable. The yield criterion is postulated in terms of effective quantities, since only the continuous, non-damaged part of the volume is undergoing plastic deformations. The stationarity conditions associated to the (effective) principle of maximum dissipation provide the *effective elastoplastic evolution laws*:

$$\dot{\boldsymbol{\varepsilon}}^p = \dot{\lambda}\,\partial_{\sigma_0} f_y \quad , \quad \dot{\alpha} = -\dot{\lambda}\,\partial_{\chi_0} f_y \quad , \quad \dot{\lambda} \geq 0 \quad , \quad f_y \leq 0 \quad , \quad \dot{\lambda}\, f_y = 0 \tag{7}$$

where $\dot{\lambda}$ is the non-negative rate of a scalar plastic multiplier. Finally, the ductile-fracture specific dissipation rate $\dot{\phi}^{pf}$ reads:

$$\dot{\phi}^{pf} := \omega\, \dot{\phi}_0^p + \dot{\phi}^f \quad , \quad \dot{\phi}^f := G\, \dot{d} \quad , \quad G := -\omega'\, \psi_0 \tag{8}$$

where the $\dot{\phi}^f$ is the brittle fracture specific dissipation rate and G is the fracture driving force. $\dot{\phi}^{pf}$ is the dissipation rate per unit nominal volume and, therefore, the elementary dissipation rate is $\dot{\phi}^{pf}\, d\Omega_0$.

2.3. Variational formulation of the finite-step problem

2.3.1. Elastoplastic variational update

Let us first consider an elastoplastic material without damage. In this case, effective and nominal quantities coincide, since there are no developing defects inside the volume. The subscript 0 will be therefore used only for homogeneity with the subsequent sections. Let Δw_0^{int} be the specific elastoplastic internal work carried out along a deformation process between time t^n and t^{n+1}

$$\Delta w_0^{int} = \int_{t^n}^{t^{n+1}} \boldsymbol{\sigma}_0 : \dot{\boldsymbol{\varepsilon}} dt = \int_{t^n}^{t^{n+1}} [\boldsymbol{\sigma}_0 : \dot{\boldsymbol{\varepsilon}}^e + \chi_0 \dot{\alpha} + (\boldsymbol{\sigma}_0 : \dot{\boldsymbol{\varepsilon}}^p - \chi_0 \dot{\alpha})]\, dt = \Delta\psi_0^e + \Delta\psi_0^p + \Delta\phi_0^p \tag{9}$$

where the symbol $\Delta(\cdot)$ denotes the increment of the quantity $(\cdot)$ over the time step $\Delta t = t^{n+1} - t^n$. We define an extremal path as a path in strain space from $\boldsymbol{\varepsilon}^n = \boldsymbol{\varepsilon}(t^n)$ to $\boldsymbol{\varepsilon}^{n+1} = \boldsymbol{\varepsilon}(t^{n+1})$, $\boldsymbol{\varepsilon}^n$ and $\boldsymbol{\varepsilon}^{n+1}$ being prescribed strains, minimizing the internal work Δw_0^{int}. Let $\Delta \bar{w}_0^{int}$ be the minimum value of Δw_0^{int}, so that $\Delta w_0^{int} \geq \Delta \bar{w}_0^{int}$ along any strain path from $\boldsymbol{\varepsilon}^n$ to $\boldsymbol{\varepsilon}^{n+1}$.

Since $\Delta\psi_0^e$ and $\Delta\psi_0^p$ are path independent quantities, they take the same value along any path between $\boldsymbol{\varepsilon}^n$ and $\boldsymbol{\varepsilon}^{n+1}$ and the extremal path minimizes $\Delta\phi_0^p$. Let $\Delta\bar{\phi}_0^p$ be this minimum value. Obviously, if a feasible purely elastic path exists from $\boldsymbol{\varepsilon}^n$ to $\boldsymbol{\varepsilon}^{n+1}$, this is an extremal path. While the sum $\Delta\boldsymbol{\varepsilon} = \boldsymbol{\varepsilon}^{n+1} - \boldsymbol{\varepsilon}^n = \Delta\boldsymbol{\varepsilon}^e + \Delta\boldsymbol{\varepsilon}^p$ is prescribed, different paths lead to different increments of elastic and plastic strains. The extremal path is therefore the solution of the following minimization problem:

$$\Delta \bar{w}_0^{int} = \min_{\Delta\boldsymbol{\varepsilon}^e, \Delta\boldsymbol{\varepsilon}^p, \Delta\alpha} \{\Delta\psi_0^e + \Delta\psi_0^p + \Delta\phi_0^p \mid \Delta\boldsymbol{\varepsilon}^e + \Delta\boldsymbol{\varepsilon}^p = \Delta\boldsymbol{\varepsilon}\} \tag{10}$$

where the total strain increment $\Delta\boldsymbol{\varepsilon}$ is prescribed.

Based on the principle of maximum dissipation, it has been shown [23, 24] that, for prescribed increments of $\Delta\boldsymbol{\varepsilon}^p$ and $\Delta\alpha$ over the time step, extremal paths in the plastic variables space (i.e., leading to the minimum increment of dissipation $\Delta\bar{\phi}_0^p$) are obtained by letting $\boldsymbol{\varepsilon}^p$ and α evolve only at constant stress, as it is the case when a backward-difference time integration of the elastoplastic constitutive law (often referred to as *return mapping algorithm*) is adopted. In this case, the step can be seen to have been elastic until the end of the step and plastic evolution is allowed only when the final values $\boldsymbol{\sigma}_0^{n+1}$ and χ_0^{n+1} have been achieved (see [28] for a review of extremum properties of the generalized midpoint time integration rule). The backward-difference integrated conditions defining the extremal path, i.e. its optimality conditions, are given by (with $f_y^{n+1} = f_y(\boldsymbol{\sigma}_0^{n+1}, \chi_0^{n+1})$):

$$\Delta\boldsymbol{\varepsilon}^p = \Delta\lambda\, \partial_{\sigma_0} f_y^{n+1} \quad , \quad \Delta\alpha = -\Delta\lambda\, \partial_{\chi_0} f_y^{n+1} \quad , \quad \Delta\lambda \geq 0 \quad , \quad f_y^{n+1} \leq 0 \quad , \quad \Delta\lambda \cdot f_y^{n+1} = 0 \tag{11}$$

while the backward-difference finite-step version of the principle of maximum dissipation reads

$$\Delta\bar{\phi}_0^p = \max_{\boldsymbol{\sigma}_0^{n+1}, \chi_0^{n+1} \in f_y \leq 0} \{\boldsymbol{\sigma}_0^{n+1} : \Delta\boldsymbol{\varepsilon}^p - \chi_0^{n+1}\Delta\alpha\} \tag{12}$$

For the considered class of generalized standard materials, the backward-difference integration algorithm has also been shown to preserve the symmetry of the consistent tangent, implying the existence of an incremental potential $\bar{w}_0^{int\,n}$ such that $\boldsymbol{\sigma}_0^{n+1} = \partial\bar{w}_0^{int\,n} / \partial\boldsymbol{\varepsilon}^{n+1}$ [24]. In view of the special extremal property of the backward-difference integrated elastoplastic constitutive law, this time-integration scheme will be adopted throughout this work and the symbol $\Delta\phi_0^p$ (without the bar) will be used to denote its corresponding plastic dissipation increment over the time step. Assuming that the solution of the elastoplastic problem is known at time t^n, this choice of the integration scheme allows for a variational characterization of the solution of the finite-step elastoplastic problem, which can be shown to coincide with the solution of the following constrained minimization problem [26, 27, 28]:

$$\min_{\mathbf{u},\Delta\boldsymbol{\varepsilon}}\left\{\Pi_p^n = \int_{\Omega_0}\left(\psi_0^{n+1} + \Delta\phi_0^p\right) d\Omega_0 - \mathcal{W}^{n+1}\right\} \tag{13}$$

where

$$\psi_0^{n+1} = \psi_0^e\left(\boldsymbol{\varepsilon}^{e\,n} + \Delta\boldsymbol{\varepsilon}^e\right) + \psi_0^p\left(\alpha^n + \Delta\alpha\right) \tag{14}$$

$\mathcal{W}$ denotes the external work and the functional is subjected to the compatibility conditions

$$\boldsymbol{\varepsilon}^n + \Delta\boldsymbol{\varepsilon}^e + \Delta\boldsymbol{\varepsilon}^p = \boldsymbol{\varepsilon}^{n+1} = \boldsymbol{\nabla}^s\mathbf{u}^{n+1}, \quad \mathbf{u}^{n+1} = \bar{\mathbf{u}}^{n+1} \text{ on } \partial\Omega_D \tag{15}$$

$\bar{\mathbf{u}}^{n+1}$ being prescribed displacement values at $t = t^{n+1}$ on the constrained boundary $\partial\Omega_D$. In (13), $\Delta\phi_0^p$ is the extremal dissipation increment resulting from application of the return mapping algorithm.

The minimum problem in (13) can be expressed in a more explicit form by writing its associated Lagrangian functional [25, 29]:

$$\begin{aligned}\mathcal{L}_p^n(\mathbf{u}^{n+1}, \Delta\boldsymbol{\varepsilon}^e, \Delta\boldsymbol{\varepsilon}^p, \Delta\alpha, \boldsymbol{\sigma}_0^{n+1}, \Delta\lambda) = \Pi_p^n - \int_{\Omega_0} f_y\left(\Delta\boldsymbol{\varepsilon}^e,\, \Delta\alpha\right)\Delta\lambda\, d\Omega_0 - \\ - \int_{\Omega_0}\boldsymbol{\sigma}_0^{n+1} : \left[\boldsymbol{\varepsilon}^{e\,n} + \boldsymbol{\varepsilon}^{p\,n} + \Delta\boldsymbol{\varepsilon}^e + \Delta\boldsymbol{\varepsilon}^p - \boldsymbol{\nabla}^s\mathbf{u}^{n+1}\right] d\Omega_0,\end{aligned} \tag{16}$$

subject to $\Delta\lambda \geq 0$ and $\mathbf{u}^{n+1} = \bar{\mathbf{u}}^{n+1}$ on $\partial\Omega_D$.

In (16), $\boldsymbol{\sigma}_0^{n+1}$ (not sign-constrained) and $\Delta\lambda \geq 0$ play the role of Lagrange multipliers for the compatibility and plastic admissibility constraints. It is easy to verify that the solution of the finite-step elastoplastic boundary value problem is given by the solution of the following variational problem, where the last condition is a variational inequality due to the sign constraint on $\Delta\lambda$:

$$\begin{aligned}
&\partial_{\mathbf{u}}\mathcal{L}_p^n[\delta\mathbf{u}] = 0 && \forall\,\delta\mathbf{u},\ \text{with } \delta\mathbf{u} = 0 \text{ on } \partial\Omega_D\\
&\partial_{\Delta\boldsymbol{\varepsilon}^e}\mathcal{L}_p^n[\delta\Delta\boldsymbol{\varepsilon}^e] = 0 && \forall\,\delta\Delta\boldsymbol{\varepsilon}^e\\
&\partial_{\Delta\boldsymbol{\varepsilon}^p}\mathcal{L}_p^n[\delta\Delta\boldsymbol{\varepsilon}^p] = 0 && \forall\,\delta\Delta\boldsymbol{\varepsilon}^p\\
&\partial_{\Delta\alpha}\mathcal{L}_p^n[\delta\Delta\alpha] = 0 && \forall\,\delta\Delta\alpha\\
&\partial_{\sigma_0}\mathcal{L}_p^n[\delta\boldsymbol{\sigma}_0^{n+1}] = 0 && \forall\,\delta\boldsymbol{\sigma}_0^{n+1}\\
&\partial_{\Delta\lambda}\mathcal{L}_p^n[\delta\lambda] \geq 0 && \forall\,\delta\lambda = \Delta\lambda' - \Delta\lambda,\ \text{with } \Delta\lambda' \geq 0 \text{ and } \Delta\lambda \geq 0
\end{aligned} \tag{17}$$

2.3.2. Phase-field finite-step variational formulation of ductile fracture

To account for the propagation of fracture driven by the development of localized plasticity, the functional $\mathcal{L}_p^n$ in (16) is enriched by the addition of the energy dissipated by the damage-like phase field d, responsible for the material stiffness and strength degradation. Since in the presence of softening structural response plastic strains tend to localize in a zero-thickness band, a further regularization of the model becomes necessary (see, e.g., [10, 19, 12, 13, 20]). A common and effective provision, motivated by microscale considerations (see, e.g., [39, 40]) consists in introducing into the model a diffusive term of an inelastic, irreversible quantity (see, e.g., [41, 42]). The simple and effective gradient formulation of finite-step elastoplasticity presented in [32] is considered here. Defining the set

$$\mathcal{S} := (\mathbf{u}, \boldsymbol{\varepsilon}, \Delta\boldsymbol{\varepsilon}^p, \boldsymbol{\sigma}_0, \boldsymbol{\sigma}_0^p, \chi_0, \Delta\alpha, \Delta\lambda, \Delta d) \tag{18}$$

of independent fields, the new, gradient-enriched functional $\mathcal{L}_{pd}^{\nabla\, n}(\mathcal{S})$ is defined below. The stress field $\boldsymbol{\sigma}_0^p$ in $\mathcal{S}$ is a dummy field considered to facilitate the derivation of the governing equations resulting from the stationarity of the functional. For all quantities evaluated at time t^{n+1}, the $n+1$ at exponent has been omitted for notation convenience:

$$\begin{aligned}
\mathcal{L}_{pd}^{\nabla\, n} :=\; & \underbrace{\int_{\Omega_0} \omega(d) \left[\psi_0^e(\boldsymbol{\varepsilon} - \boldsymbol{\varepsilon}^{p\,n} - \Delta\boldsymbol{\varepsilon}^p) + \psi_0^p(\alpha^n + \Delta\alpha)\right] \mathrm{d}\Omega_0}_{stored\ \ internal\ \ energy\ \ \mathcal{E}} - \underbrace{\int_{\Omega_0} \mathbf{b}\cdot\mathbf{u}\,\mathrm{d}\Omega_0 - \int_{\partial\Omega_N} \mathbf{t}\cdot\mathbf{u}\,\mathrm{d}\Gamma}_{external\ \ work\ \ \mathcal{W}} + \\
& + \underbrace{\int_{\Omega_0} \omega(d) \left(\boldsymbol{\sigma}_0^p : \Delta\boldsymbol{\varepsilon}^p - \chi_0\,\Delta\alpha\right) \mathrm{d}\Omega_0}_{plastic\ \ dissipation\ \ increment\ \ \Delta\mathcal{D}^p} + \underbrace{\int_{\Omega_0} \phi^f(d, \boldsymbol{\nabla} d)\,\mathrm{d}\Omega_0}_{fracture\ \ energy\ \ \mathcal{D}_f} + \underbrace{\int_{\Omega_0} \frac{\eta_f}{2\,\Delta t}\,(\Delta d)^2\,\mathrm{d}\Omega_0}_{viscous\ \ energy\ \ \mathcal{D}_v} + \\
& + \underbrace{\int_{\Omega_0} \omega(d)\,\boldsymbol{\sigma}_0 : (\boldsymbol{\nabla}^s\mathbf{u} - \boldsymbol{\varepsilon})\,\mathrm{d}\Omega_0}_{compatibility\ \ constraint} - \underbrace{\int_{\Omega_0} \omega(d)\,\Delta\lambda\, f_y(\boldsymbol{\sigma}_0^p, \chi_0)\,\mathrm{d}\Omega_0 + \int_{\Omega_0} \omega(d)\,\frac{1}{2}\,c_p\,\boldsymbol{\nabla}\lambda\cdot\boldsymbol{\nabla}\lambda\,\mathrm{d}\Omega_0}_{plastic\ \ admissibility}
\end{aligned} \tag{19}$$

subject to

$$\Delta\lambda \geq 0, \quad \Delta d \geq 0, \quad \mathbf{u} = \bar{\mathbf{u}} \text{ on } \partial\Omega_D \tag{20}$$

The notion of effective volume enters in the definition of the volume integrals. With the exception of the fracture energy $\mathcal{D}_f$ and of the external work $\mathcal{W}$, the energies and the constraints are defined on the continuous portion of the material volume Ω only, hence $\int_\Omega (\cdot)_0\,\mathrm{d}\Omega = \int_{\Omega_0} \omega\,(\cdot)_0\,\mathrm{d}\Omega_0$, Ω_0 being the reference nominal volume. The vectors $\mathbf{b}$ and $\mathbf{t}$ are the body forces and the tractions, respectively, applied on the Neumann portion $\partial\Omega_N$ of the boundary. In the standard phase-field formulation,

$$\phi^f(d, \boldsymbol{\nabla} d) = w(d) + {}^1\!/\!{}_2\, c_d\,\boldsymbol{\nabla} d\cdot\boldsymbol{\nabla} d \tag{21}$$

where $w(d)$ is the local phase-field specific dissipation. The constant parameters c_p and c_d measure the plastic and damage diffusion bandwidths and they are related to the plastic and fracture internal lengths l_{0p} and l_{0d}. The viscous coefficient η_f introduces a pseudo-time measure of the crack propagation rate, while $\Delta t = t^{n+1} - t^n$ is the current time-step size. This dissipative term is introduced for algorithmic reasons, as it will be discussed later. The solution of the considered ductile fracture boundary value problem makes the functional $\mathcal{L}_{pd}^{\nabla\, n}(\mathcal{S})$ stationary with respect to variations of the fields in $\mathcal{S}$. The inequality constraints on $\Delta\lambda$ and Δd make the variational problem a variational inequality.

2.3.3. Stationarity conditions

The stationarity conditions for $\mathcal{L}_{pd}^{\nabla\, n}(\mathcal{S})$ read:

$$\partial_{\mathbf{u}}\mathcal{L}_{pd}^{\nabla\, n}(\mathcal{S})[\delta\mathbf{u}] = 0 \quad \rightarrow \quad \int_{\Omega_0} \omega\, \boldsymbol{\sigma}_0 : \boldsymbol{\nabla}^s\delta\mathbf{u}\, \mathrm{d}\Omega_0 - \int_{\Omega_0} \mathbf{b}\cdot\delta\mathbf{u}\,\mathrm{d}\Omega_0 - \int_{\partial\Omega_N} \mathbf{t}\cdot\delta\mathbf{u}\,\mathrm{d}\Gamma = 0 \tag{22a}$$

$$\partial_{\boldsymbol{\varepsilon}}\mathcal{L}_{pd}^{\nabla\, n}(\mathcal{S})[\delta\boldsymbol{\varepsilon}] = 0 \quad \rightarrow \quad \int_{\Omega_0} \omega\left(\partial_{\boldsymbol{\varepsilon}}\psi_0^e - \boldsymbol{\sigma}_0\right) : \delta\boldsymbol{\varepsilon}\,\mathrm{d}\Omega_0 = 0 \tag{22b}$$

$$\partial_{\boldsymbol{\sigma}_0}\mathcal{L}_{pd}^{\nabla\, n}(\mathcal{S})[\delta\boldsymbol{\sigma}_0] = 0 \quad \rightarrow \quad \int_{\Omega_0} \omega\left(\boldsymbol{\nabla}^s\mathbf{u} - \boldsymbol{\varepsilon}\right) : \delta\boldsymbol{\sigma}_0\,\mathrm{d}\Omega_0 = 0 \tag{22c}$$

$$\partial_{\alpha}\mathcal{L}_{pd}^{\nabla\, n}(\mathcal{S})[\delta\alpha] = 0 \quad \rightarrow \quad \int_{\Omega_0} \omega\left(\partial_{\alpha}\psi_0^p - \chi_0\right)\delta\alpha\,\mathrm{d}\Omega_0 = 0 \tag{22d}$$

$$\partial_{\boldsymbol{\varepsilon}^p}\mathcal{L}_{pd}^{\nabla\, n}(\mathcal{S})[\delta\boldsymbol{\varepsilon}^p] = 0 \quad \rightarrow \quad \int_{\Omega_0} \omega\left(-\partial_{\boldsymbol{\varepsilon}}\psi_0^e + \boldsymbol{\sigma}_0^p\right) : \delta\boldsymbol{\varepsilon}^p\,\mathrm{d}\Omega_0 = 0 \tag{22e}$$

$$\partial_{\boldsymbol{\sigma}_0^p}\mathcal{L}_{pd}^{\nabla\, n}(\mathcal{S})[\delta\boldsymbol{\sigma}_0^p] = 0 \quad \rightarrow \quad \int_{\Omega_0} \omega\left(\Delta\boldsymbol{\varepsilon}^p - \Delta\lambda\,\partial_{\boldsymbol{\sigma}_0^p} f_y\right) : \delta\boldsymbol{\sigma}_0^p\,\mathrm{d}\Omega_0 = 0 \tag{22f}$$

$$\partial_{\chi_0}\mathcal{L}_{pd}^{\nabla\, n}(\mathcal{S})[\delta\chi_0] = 0 \quad \rightarrow \quad \int_{\Omega_0} -\omega\left(\Delta\alpha + \Delta\lambda\,\partial_{\chi_0} f_y\right)\delta\chi_0\,\mathrm{d}\Omega_0 = 0 \tag{22g}$$

$$\partial_{\lambda}\mathcal{L}_{pd}^{\nabla\, n}(\mathcal{S})[\delta\lambda] \geq 0 \quad \rightarrow \quad \int_{\Omega_0} \omega\left[-\delta\lambda\, f_y + c_p\,\boldsymbol{\nabla}\lambda\cdot\boldsymbol{\nabla}\delta\lambda\right]\mathrm{d}\Omega_0 \geq 0 \tag{22h}$$

$$\partial_{d}\mathcal{L}_{pd}^{\nabla\, n}(\mathcal{S})[\delta d] \geq 0 \quad \rightarrow \quad \int_{\Omega_0} \left\{\left[\omega'\,\tilde{\psi}_0 + w' + \frac{\eta_f}{\tau}\,\Delta d\right]\delta d + c_d\,\boldsymbol{\nabla}d\cdot\boldsymbol{\nabla}\delta d\right\}\mathrm{d}\Omega_0 \geq 0, \tag{22i}$$

where $\delta\lambda = \Delta\lambda' - \Delta\lambda$, $\delta d = \Delta d' - \Delta d$ are not sign-constrained, while $\Delta\lambda' \geq 0$, $\Delta d' \geq 0$ are aribitrary, non-negative scalar functions belonging to the same spaces of $\Delta\lambda$ and Δd, respectively, and

$$\Delta\lambda \geq 0, \quad \Delta d \geq 0, \quad \mathbf{u} = \bar{\mathbf{u}} \text{ on } \partial\Omega_D$$

The driving energy $\tilde{\psi}_0$ in (22i) is defined as

$$\tilde{\psi}_0(\boldsymbol{\varepsilon}, \boldsymbol{\varepsilon}^p, \boldsymbol{\sigma}_0^p, \chi_0, \alpha, \lambda) := \psi_0(\boldsymbol{\varepsilon}, \boldsymbol{\varepsilon}^p, \alpha) + \Delta\phi_0^p(\boldsymbol{\varepsilon}^p, \boldsymbol{\sigma}_0^p, \chi_0, \alpha) - f_y(\boldsymbol{\sigma}_0^p, \chi_0)\,\Delta\lambda + {}^1\!/\!_2\, c_p\,\boldsymbol{\nabla}\lambda\cdot\boldsymbol{\nabla}\lambda \tag{23}$$

It contains the term $f_y\,\Delta\lambda$ that is non-vanishing due to the gradient plasticity term. The conditions above correspond to: (22a) equilibrium equations, (22b) elastic state equations, (22c) compatibility conditions, (22d) static hardening variable state equation, (22e) (together with (22b)) identity between the dummy stress $\boldsymbol{\sigma}_0^p$ and the effective stress $\boldsymbol{\sigma}_0$, (22f) plastic strains evolution, (22g) hardening variable evolution, (22h) non-local plastic consistency, (22i) non-local fracture evolution criterion. To simplify the notation in what follows, the symbols α, λ, d are used to express the functional dependencies, rather than the corresponding increments $\Delta\alpha, \Delta\lambda, \Delta d$ as already done in (23).

2.3.4. Governing equations of the non-local problem

In the implemented formulation, the compatibility condition (22c) is enforced in strong form, i.e. $\boldsymbol{\varepsilon} = \boldsymbol{\nabla}_s\mathbf{u}$ as in standard compatible finite elements, and the dummy stress field $\boldsymbol{\sigma}_0^p$ is eliminated assuming $\boldsymbol{\sigma}_0^p \equiv \boldsymbol{\sigma}_0$. Equation (22a), combined with the compatibility condition (22c), leads to the weak form of the momentum balance equation, expressed in terms of nominal quantities:

$$\int_{\Omega_0} \omega\,\boldsymbol{\sigma}_0 : \delta\boldsymbol{\varepsilon}\,\mathrm{d}\Omega_0 = \int_{\Omega_0} \mathbf{b}\cdot\delta\mathbf{u}\,\mathrm{d}\Omega_0 + \int_{\partial\Omega_N} \mathbf{t}\cdot\delta\mathbf{u}\,\mathrm{d}\Gamma \tag{24}$$

The stationarity conditions (22b), (22d)-(22g), lead to the effective local state equations and elastoplastic evolution laws:

$$\boldsymbol{\sigma}_0 = \partial_{\boldsymbol{\varepsilon}}\psi_0^e \quad , \quad \chi_0 = \partial_\alpha\psi_0^p \quad , \quad \Delta\boldsymbol{\varepsilon}^p = \Delta\lambda\,\partial_{\boldsymbol{\sigma}_0} f_y \quad , \quad \Delta\alpha = -\Delta\lambda\,\partial_{\chi_0} f_y \tag{25}$$

while the corresponding nominal stress and static internal variable are obtained as $\boldsymbol{\sigma} = \omega\boldsymbol{\sigma}_0$, $\chi = \omega\chi_0$.

While the variations (22a)-(22g) are standard equalities, (22h) and (22i) are variational inequalities. Using standard arguments for variational inequalities, condition (22h) can be written in the following equivalent form defining the elastoplastic non-local loading-unloading conditions:

$$\Delta\lambda \geq 0 \quad , \quad \mathcal{F}_y(\boldsymbol{\sigma}_0, \chi_0, \lambda, d) \leq 0 \quad , \quad \mathcal{F}_y(\boldsymbol{\sigma}_0, \chi_0, \lambda, d)[\Delta\lambda] = 0 \tag{26}$$

where the non-local yield functional $\mathcal{F}_y$ has been defined as:

$$\mathcal{F}_y(\boldsymbol{\sigma}_0, \chi_0, \lambda, d)[\delta\lambda] := \int_{\Omega_0} \omega(d)\left[\, f_y(\boldsymbol{\sigma}_0, \chi_0)\,\delta\lambda - c_p\,\boldsymbol{\nabla}\lambda\cdot\boldsymbol{\nabla}\delta\lambda\,\right]\mathrm{d}\Omega_0 \tag{27}$$

Similarly, the energy release rate $\mathcal{G}$ and critical energy release rate $\mathcal{G}_c$ functionals are defined as:

$$\mathcal{G}(\boldsymbol{\varepsilon}, \boldsymbol{\varepsilon}^p, \alpha, \lambda, d)[\delta d] := -\int_{\Omega_0} \omega'(d)\,\tilde{\psi}_0(\boldsymbol{\varepsilon}, \boldsymbol{\varepsilon}^p, \alpha, \lambda)\,\delta d\,\mathrm{d}\Omega_0 \tag{28a}$$

$$\mathcal{G}_c(d)[\delta d] := \int_{\Omega_0} \left\{ \left[w'(d) + \frac{\eta_f}{\tau}\,\Delta d \right] \delta d + c_d\,\boldsymbol{\nabla}d\cdot\boldsymbol{\nabla}\delta d \right\} \mathrm{d}\Omega_0 \tag{28b}$$

where the evolution laws (25) have been used to reduce the number of independent fields in the driving energy $\tilde{\psi}_0$. The non-local fracture activation functional $\mathcal{F}_d$ is then defined as:

$$\mathcal{F}_d(\boldsymbol{\varepsilon}, \boldsymbol{\varepsilon}^p, \alpha, \lambda, d)[\delta d] := \Big(\mathcal{G}(\boldsymbol{\varepsilon}, \boldsymbol{\varepsilon}^p, \alpha, \lambda, d) - \mathcal{G}_c(d)\Big)[\delta d] \tag{29}$$

and condition (22i) is rewritten in the equivalent form

$$\Delta d \geq 0 \quad , \quad \mathcal{F}_d(\boldsymbol{\varepsilon}, \boldsymbol{\varepsilon}^p, \alpha, \lambda, d) \leq 0 \quad , \quad \mathcal{F}_d(\boldsymbol{\varepsilon}, \boldsymbol{\varepsilon}^p, \alpha, \lambda, d)[\Delta d] = 0 \tag{30}$$

providing the non-local fracture activation criterion for elastoplastic brittle fracture. It should be noted that in this elastoplastic-brittle-fracture model the only coupling between plastic and fracture dissipation mechanisms is present in the fracture driving force $\mathcal{G}$, while the fracture dissipation $\mathcal{G}_c$ is the same as the one of the purely brittle case.

2.4. Constitutive assumptions

For the implementation considered in this work, the general framework described so far is restricted to isotropic linear elastic materials, obeying von Mises plasticity criterion with linear isotropic hardening, i.e.

$$\psi_0^e(\boldsymbol{\varepsilon} - \boldsymbol{\varepsilon}^p) = {}^1\!/\!_2\, K_0\, \epsilon_v^2 + {}^1\!/\!_2\, 2G_0\, (\mathbf{e} - \boldsymbol{\varepsilon}^p) : (\mathbf{e} - \boldsymbol{\varepsilon}^p), \quad f_y(\mathbf{s}_0, \chi_0) = \sqrt{{}^3\!/\!_2\, \mathbf{s}_0 : \mathbf{s}_0} - \bar{\sigma}_{y0} - \chi_0 \tag{31}$$

where K_0 is the bulk modulus, G_0 is the shear modulus, $\bar{\sigma}_{y0}$ is the initial yield stress, $\epsilon_v := \boldsymbol{\varepsilon} : \mathbf{I}$ is the total volumetric strain, $\mathbf{I}$ being the identity tensor, $\mathbf{e} = \boldsymbol{\varepsilon} - {}^1\!/\!_3\epsilon_v\mathbf{I}$ is the deviatoric total strain, $\mathbf{s}_0 = \boldsymbol{\sigma}_0 - p\mathbf{I}$, is the deviatoric effective stress, p being the hydrostatic pressure (taken positive if tensile) and $\chi_0 = H_0\alpha$ is the static internal variable, H_0 being the hardening modulus. The restriction to von-Mises plasticity allows to identify the internal hardening variable α with the equivalent plastic strain and its increment is given by $\Delta\alpha = \sqrt{{}^2\!/\!_3\, \Delta\boldsymbol{\varepsilon}^p : \Delta\boldsymbol{\varepsilon}^p}$.

The phase-field functions $\omega(d)$ and $w(d)$ are defined as

$$\omega(d) = (1 - d)^2, \quad w(d) = \frac{3G_c}{8l_{0d}}\, d \tag{32}$$

where G_c is the material toughness and l_{0d} the phase-field internal length. This definition of $w(d)$ corresponds to an AT1 approach, where AT stands for AmbrosioTortorelli and the corresponding type of regularization [43], implying that damage cannot develop until a critical value of the damage driving force has been achieved. Finally, the fracture diffusion coefficient c_d of the AT1 model is defined as $c_d = {}^3\!/\!_4\, G_c\, l_{0d}$, the plastic diffusion coefficient c_p as $c_p = \sigma_0\, l_{0p}^2$, and the viscous coefficient η_f as $\eta_f = \bar{\eta}\, ({}^{G_c}\!/\!_{l_{0d}})$.

To avoid the promotion of crack propagation by predominantly compressive states, the deviatoric-volumetric elastic energy split is adopted (see, e.g. [44, 45]). According to this technique, the elastic energy is split into an *Inactive* part ψ_0^{eI}, due to negative volumetric strains, and an *Active* remainder ψ_0^{eA}, which are defined as:

$$\psi_0^{eA}(\boldsymbol{\varepsilon}, \boldsymbol{\varepsilon}^p) = {}^1\!/\!{}_2\, K_0 \, \langle \epsilon_v \rangle_+^2 + {}^1\!/\!{}_2\, 2G_0\, (\mathbf{e} - \boldsymbol{\varepsilon}^p) : (\mathbf{e} - \boldsymbol{\varepsilon}^p) \qquad , \qquad \psi_0^{eI}(\boldsymbol{\varepsilon}, \boldsymbol{\varepsilon}^p) = {}^1\!/\!{}_2\, K_0 \, \langle \epsilon_v \rangle_-^2 \tag{33}$$

where $\langle \cdot \rangle_\pm$ are the Macaulay brackets. In view of the purely deviatoric nature of plastic strains in von Mises plasticity, no distinction is made between the tensile/compressive parts of the plastic component ψ^p of the free energy density. Note that a split also of this energy component may be recommended in the presence of dilatant elastoplastic materials (see, e.g., [6] for the case of geological materials). The assumed energy split has implications on the definition of the nominal stress and of the plastic dissipation rate. Taking into account the elastic energy split, the nominal free energy is defined as

$$\psi = \omega(\psi_0^{eA} + \psi^p) + \psi_0^{eI} \tag{34}$$

and, from the dissipation inequality (3), one has that the nominal stress is given by:

$$\boldsymbol{\sigma} = \partial_{\boldsymbol{\varepsilon}^e} \psi^e = \omega\, \partial_{\boldsymbol{\varepsilon}^e} \psi_0^{eA} + \partial_{\boldsymbol{\varepsilon}^e} \psi_0^{eI} = \omega\, \boldsymbol{\sigma}_0^A + \boldsymbol{\sigma}_0^I \neq \omega\, \partial_{\boldsymbol{\varepsilon}^e} \psi_0^e = \omega\, \boldsymbol{\sigma}_0 \tag{35}$$

and no straightforward transformation from effective to nominal stress can be applied. The active and inactive effective stresses are defined:

$$\boldsymbol{\sigma}_0^A := \partial_{\boldsymbol{\varepsilon}^e} \psi_0^{eA} \quad , \quad \boldsymbol{\sigma}_0^I := \partial_{\boldsymbol{\varepsilon}^e} \psi_0^{eI} \qquad \textit{with} \qquad \boldsymbol{\sigma}_0 = \boldsymbol{\sigma}_0^A + \boldsymbol{\sigma}_0^I \tag{36}$$

However, for the considered case of von Mises plasticity and volumetric-deviatoric split, one has that $\boldsymbol{\sigma}_0^I : \dot{\boldsymbol{\varepsilon}}^p = 0$ and the plastic dissipation rate can still be defined as

$$\dot{\phi} = \boldsymbol{\sigma} : \dot{\boldsymbol{\varepsilon}}^p - \chi \dot{\alpha} = \omega\, (\boldsymbol{\sigma}_0^A : \dot{\boldsymbol{\varepsilon}}^p - \chi_0 \dot{\alpha}) = \omega\, \dot{\phi}_0 \tag{37}$$

For the case of dilatant geological materials, see also the discussion in [6].

3. Modulation of ductile-brittle interaction

The proposed approach to plasticity-driven phase-field fracture propagation is based on the definition of a non-variational scalar function $f(\alpha)$ of the equivalent plastic strain, hereafter referred to as *modulation* *function*, modulating the evolution of the critical fracture energy G_c, based on the evolution of the plastic process zone. In ductile fracture, the material resistance to crack extension grows due the growth of the plastic zone at the crack tip, until it reaches a limit value (the so-called R-curve). The critical fracture energy G_c represents this steady state value of the energy to be spent for a unit crack advancement, which however includes also the energy to be dissipated in the creation of the plastic process zone. In the considered model, this latter energy is explicitly taken into account by the plastic dissipation $\Delta\phi_0^p$.

To account for these interaction phenomena, the proposed model is based on the assumption that damage, measured by the phase-field order parameter d, can grow only when the plastic process zone in a stress concentration region has fully developed, as measured by the local value of the equivalent plastic strain α. In practical terms, the competition between the plasticity and fracture dissipation mechanisms in the initial crack nucleation phase and their interaction in the subsequent crack propagation phase, is modulated by the addition of a new non-variational interaction term in the expression of the critical energy release rate functional $\mathcal{G}_c$ (28b):

$$\mathcal{G}_c^{\alpha}(\alpha, d)[\delta d] := \underbrace{\int_{\Omega_0} f(\alpha)\, w'(d)\, \delta d \,\mathrm{d}\Omega_0}_{\textit{interaction term}} + \underbrace{\int_{\Omega_0} \left\{ \left[w'(d) + \frac{\eta_f}{\tau}\, \Delta d \right] \delta d + c_d\, \nabla d \cdot \nabla \delta d \right\} \mathrm{d}\Omega_0}_{\mathcal{G}_c(d)[\delta d]} \tag{38}$$

The definition of the modulation function $f(\alpha)$ in (38) is obtained based on the study of the one-dimensional homogeneous case.

It should be noted that the assumed plasticity-driven damage activation criterion, combined with the considered isochoric Mises plasticity model, implies that no damage can develop under a purely hydrostatic tensile stress state. Consideration of this particular failure mode would require an extension of the proposed ductile-brittle interaction model, with a specific treatment of the hydrostatic tensile stress case.

3.1. One-dimensional homogeneous case

A one-dimensional problem, with homogeneous distribution of the phase field and of plastic strains, i.e. with $\nabla d = \mathbf{0}$, $\nabla \Delta\lambda = \mathbf{0}$ and without viscosity, i.e. $\eta_f = 0$, is considered. Under these assumptions, the damage activation criterion (30) can be formulated in strong form as follows:

$$\Delta d \geq 0 \quad , \quad -\left[\omega'\,(\psi_0 + \Delta\phi_0^p) + (f+1)\,\frac{3}{8}\,\frac{G_c}{l_{0d}} \right] \leq 0 \quad , \quad \left[\omega'\,(\psi_0 + \Delta\phi_0^p) + (f+1)\,\frac{3}{8}\,\frac{G_c}{l_{0d}} \right] \Delta d = 0$$

where the definition (32) of the local part $w(d)$ of the phase-field dissipation has been used. Note that, in this simple 1D homogeneous case and thanks to the absence of the gradient of the plastic multiplier, the complementarity condition $f_y \Delta\lambda = 0$ holds in strong form and, therefore, does not appear in the driving energy (23), which is simply given by $\tilde{\psi}_0 = \psi_0 + \Delta\phi_0^p$. When the phase field is evolving, i.e., when $\Delta d > 0$, and for $\omega(d) = (1-d)^2$, the activation criterion yields:

$$2(1-d)\,(\psi_0 + \Delta\phi_0^p) - (f+1)\,\frac{3}{8}\,\frac{G_c}{l_{0d}} = 0$$

where the free energy ψ_0 is defined in (2) and the increment of plastic dissipation $\Delta\phi_0^p$ in (12). Defining

$$\bar{g} := \frac{3}{16}\,\frac{G_c}{l_{0d}} \tag{39}$$

the damage activation condition can be written as:

$$\underbrace{(1-d)\,(\psi_0 + \Delta\phi_0^p)}_{\textit{driving force}} \quad - \quad \underbrace{(f+1)\,\bar{g}}_{\textit{effective fracture energy}} \quad = 0 \tag{40}$$

From this equation one can obtain the value of the phase-field variable d for prescribed displacement and plastic deformation. The point of view is now reversed. Let us assume that a damage evolution is prescribed, such that damage is zero until a critical value α_{cr} of the equivalent plastic strain is achieved and that, after this, a fictitious evolution $\bar{d}(\alpha)$ is prescribed, so that (40) can be solved for $f(\alpha) + 1$. For $\alpha \le \alpha_{cr}$, $f(\alpha)$ should be a non-decreasing function of the equivalent plastic strain α, since it is intended to account for the plastic dissipation. As a consequence, $\psi_0(\alpha)$ in (40) should also be intended as a function that can only increase in time.

To account for all these different aspects, the following form of the modulation function $f(\alpha)$ has been implemented:

$$f + 1 = \begin{cases} f_0 & \text{if} \quad \alpha = 0 \\ \frac{\tilde{\mathcal{H}}}{\bar{g}} & \text{if} \quad \alpha \le \alpha_{cr} \\ (1-\bar{d})\,\frac{\tilde{\mathcal{H}}}{\bar{g}} + (f_{min}+1)\,\bar{d} & \text{if} \quad \alpha_{cr} < \alpha < \alpha_{cr} + \Delta\alpha_{cr} \\ f_{min} + 1 & \text{if} \quad \alpha_{cr} + \Delta\alpha_{cr} \le \alpha \end{cases} \tag{41}$$

where f_0 is an initial value to be defined later and the history function $\tilde{\mathcal{H}}$ is defined as:

$$\tilde{\mathcal{H}} := \mathcal{H} + \psi_0^p + \Delta\phi_0^p - f_y\,\Delta\lambda + {}^1\!/_2\, c_p\, \nabla\lambda \cdot \nabla\lambda \tag{42}$$

with the *history variable* $\mathcal{H}$, inspired to the one in [46], defined as:

$$\mathcal{H} = \max\left(\psi_0^e, \mathcal{H}^n\right) \tag{43}$$

For $\alpha < \alpha_{cr}$, this last condition ensures that in the case of elastic unloading, i.e., $\psi_0^e < \psi_0^{en}$, the modulation function cannot decrease. Finally, $\Delta\alpha_{cr}$ defines the increment of $\alpha > \alpha_{cr}$ beyond which $f(\alpha)$ achieves its minimum constant value f_{min}, corresponding to the purely brittle portion of G_c, in the sense specified before. According to the definition (41) of $f(\alpha)$, after damage activation (i.e., for $\alpha > \alpha_{cr}$) the evolution of $f(\alpha)$ is governed by the fictitious phase-field history $\bar{d}(\alpha)$ in (41), whose definition is provided analytically in the form

$$\bar{d}(\alpha) = \begin{cases} 0 & \alpha \leq \alpha_{cr} \\ \xi^3\,(10 - 15\,\xi + 6\,\xi^2) & \alpha_{cr} < \alpha < \alpha_{cr} + \Delta\alpha_{cr} \end{cases} \qquad \xi := \frac{\alpha - \alpha_{cr}}{\Delta\alpha_{cr}} \tag{44}$$

To better understand the effect of the different parameters in the modulation function $f(\alpha)$ in (41) and of the prescribed phase-field history $\bar{d}(\alpha)$ in (44), the proposed ductile-brittle phase-field approach has been applied to a single 4-node element under a uniaxial imposed displacement in plane strain conditions, with the results shown in Figure 2 and 3. The element side is $L = 0.01\,mm$. The element is loaded by $n_{st} = 100$ equal time steps of imposed vertical displacement $\Delta u = 0.01\,mm$. The used elastoplastic material properties are those shown in Table 1 for Material II. The toughness is changed to the value $G_c = 100\,N/mm$ and the damage internal length is $l_{0d} = 1\,mm$. Since the element size is much smaller then the plasticity and damage characteristic lengths, the resulting fields will be uniform over the element. The viscous coefficient is set to $\bar{\eta} = 10^{-2}\,s$. Three material parameters have been introduced in (41): the critical equivalent plastic strain α_{cr}, i.e., a scalar measure of the plastic deformation corresponding to the onset of damage; the minimum value f_{min} of the modulation function; the plastic deformation increment $\Delta\alpha_{cr}$, beyond which the modulation function $f(\alpha)$ attains its minimum constant value f_{min}. Though a precise definition of f_{min} appears difficult, numerical tests have shown that its influence on the overall response is minor and that it affects mainly the final part of the response curve, when the structure has almost completely failed. In the considered tests, $f_{min} = 0$ has been used obtaining accurate results. It is important to remark that the condition $\alpha_{cr} > 0$ together with the AT1 assumption ensures the existence of a purely elastoplastic stage before the start of damage.

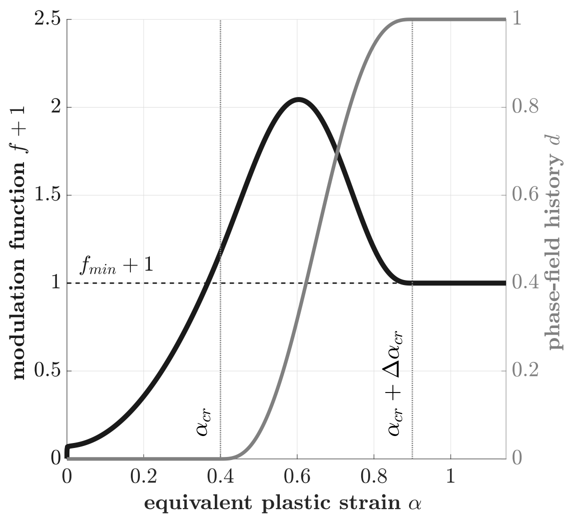

Figure 2: Modulation function $f(\alpha) + 1$ and fictitious phase-field history $\bar{d}(\alpha)$. The model parameters are $\alpha_{cr} = 0.4$, $\Delta\alpha_{cr} = 0.5$, and $f_{min} = 0$.

The profile of the modulation function $f(\alpha)$ and of the fictitious phase-field history $\bar{d}(\alpha)$ are shown in Figure 2. The initial value $f_0 + 1$ corresponds to the first yielding at the considered material point, i.e., it is given by equation (41) with $\bar{d} = 0$, $\Delta\phi_0^p = 0$, $\Delta\lambda = 0$ and ψ_0 equal to its value at the yield limit, and therefore is not a model parameter. A very important feature of the proposed form of the modulation function $f(\alpha)$ is that its evolution is given by the current value of $\tilde{\mathcal{H}}$ in (41), and does not require to be defined a priori. Therefore, in a multi-dimensional case, for $\alpha \leq \alpha_{cr}$ the function $f(\alpha)$ is computed from (41), with $\bar{d} = 0$, based on the current values of $\mathcal{H}$, ψ_0^p, $\Delta\phi_0^p$, and $\Delta\lambda$. For $\alpha \geq \alpha_{cr}$, $\bar{d}$ starts to grow, as specified in (44). At a certain point, the growth of $\bar{d}$ prevails on the other terms in (41), reducing $\mathcal{G}_c^{\alpha}(\alpha, d)$ in (38), thus allowing damage to propagate. The $f(\alpha) + 1$ curve reaches a maximum value $f_{max} + 1$ and then decreases to a minimum value $f_{min} + 1$.

The effect of the material parameters α_{cr} and $\Delta\alpha_{cr}$ is shown in Figure 3 for $f_{min} = 0$. The elastoplastic hardening response curve (without damage) is in light gray, while the orange dashed line shows the elastoplastic-brittle response, obtained without the modulation function (i.e. with $f \equiv 0$). It can be clearly noticed how in this latter model there are no parameters to be tuned to better reproduce the material response. In contrast, the introduction of the modulation function allows to achieve the two objectives mentioned before: the competition between the plastic and fracture dissipation mechanisms is modulated by tuning α_{cr} (Figure 3a), while the interaction between the two mechanisms in the failure phase is modulated by tuning $\Delta\alpha_{cr}$ (Figure 3b). α_{cr} delays the beginning of the softening branch, while $\Delta\alpha_{cr}$ controls its slope.

From Figure 3a it appears that α_{cr} should not be smaller than the value corresponding to the onset of damage in the $f \equiv 0$ case. The choice of f_{min} has a minor influence on the response. $f_{min} = 0$ corresponds to an activation criterion without the effect of the modulation function as in the elastoplastic-brittle case, i.e., the usual value of G_c is fully recovered in the final phase of the rupture process.

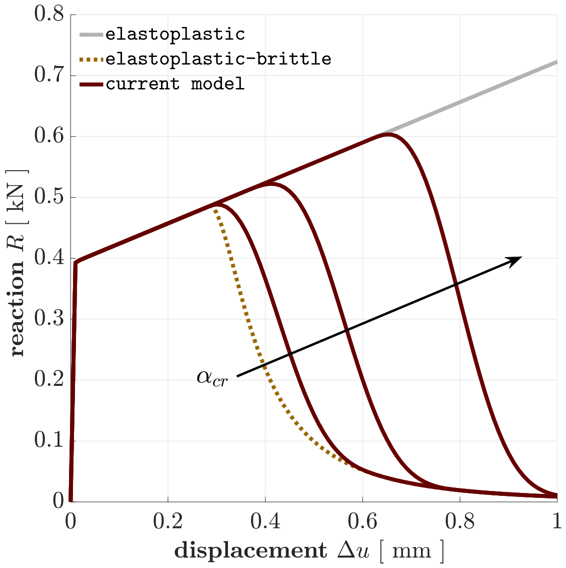

(a) Effects of α_{cr} on competition between ductile and brittle dissipation mechanisms. For fixed $\Delta\alpha_{cr} = 0.5$, the values are $\alpha_{cr} = 0.2, 0.4, 0.7$.

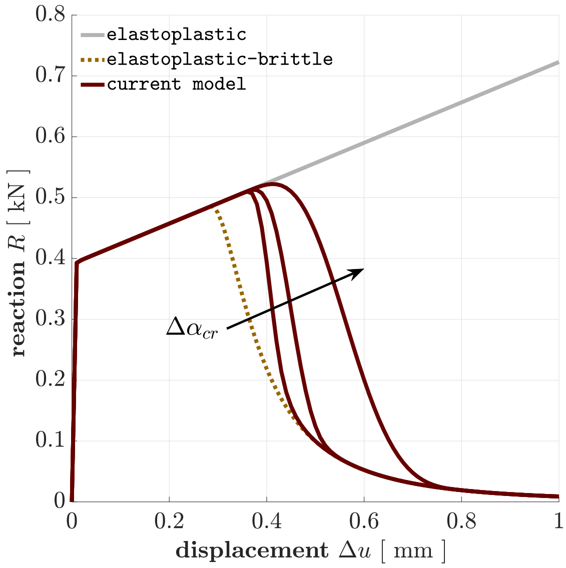

(b) Effects of $\Delta\alpha_{cr}$ on ductile-brittle interaction in failure phase. For fixed $\alpha_{cr} = 0.4$, the values are $\Delta\alpha_{cr} = 0.1, 0.2, 0.5$.

Figure 3: Effects of modulation function parameters.

4. Space discretization

The problem physical dimension is n_{dim}, the element number of nodes is n_{en}, the element number of displacement degrees of freedom is $n_{ldof} = n_{dim}\, n_{en}$. The global number of nodes is n_{np} and the global number of displacement degrees of freedom is $n_{dof} = n_{dim}\, n_{np}$. The number of independent strain tensor components is n_ε. The local, elemental and global solutions of the ductile fracture problem can be cast into the column vectors:

$$\mathcal{S}_l = (\mathbf{u}, \lambda, d) \quad , \quad \mathcal{S}_e = (\hat{\mathbf{u}}_e, \hat{\boldsymbol{\lambda}}_e, \hat{\mathbf{d}}_e) \quad , \quad \mathcal{S}_g = (\hat{\mathbf{u}}, \hat{\boldsymbol{\lambda}}, \hat{\mathbf{d}}) \tag{45}$$

where $\mathbf{u}$ is the displacement vector, of dimensions $(n_{dim}, 1)$, while λ is the plastic multiplier and d is the phase field and both are scalar fields. The element nodal displacement vector $\hat{\mathbf{u}}_e$ has dimensions $(n_{ldof}, 1)$, the element multiplier vector $\hat{\boldsymbol{\lambda}}_e$ has dimensions $(n_{en}, 1)$ and the element phase-field vector $\hat{\mathbf{d}}_e$ has dimensions

$(n_{en}, 1)$. $\hat{\mathbf{u}}$ $(n_{dof}, 1)$ is the global nodal displacement vector, $\hat{\boldsymbol{\lambda}}$ $(n_{np}, 1)$ is the global nodal multiplier vector, and $\hat{\mathbf{d}}$ $(n_{np}, 1)$ is the global nodal phase-field vector. The element local solution together with the spatial gradients, i.e. the total deformation $\boldsymbol{\varepsilon}$ $(n_\varepsilon, 1)$, the plastic multiplier gradient $\boldsymbol{\nabla}\lambda$ $(n_{dim}, 1)$ and the phase-field gradient $\boldsymbol{\nabla}d$ $(n_{dim}, 1)$ are modeled at the element level as:

$$\mathbf{u} = \mathbf{N}_\mathrm{u}\, \hat{\mathbf{u}}_e \quad , \quad \lambda = \mathbf{N}_\lambda\, \hat{\boldsymbol{\lambda}}_e \quad , \quad d = \mathbf{N}_\mathrm{d}\, \hat{\mathbf{d}}_e \tag{46a}$$

$$\boldsymbol{\varepsilon} = \mathbf{B}_\mathrm{u}\, \hat{\mathbf{u}}_e \quad , \quad \boldsymbol{\nabla}\lambda = \mathbf{B}_\lambda\, \hat{\boldsymbol{\lambda}}_e \quad , \quad \boldsymbol{\nabla}d = \mathbf{B}_\mathrm{d}\, \hat{\mathbf{d}}_e \tag{46b}$$

where $\mathbf{N}_\mathrm{u}$ is the displacement shape function matrix (n_{dim}, n_{ldof}), $\mathbf{B}_\mathrm{u}$ is displacement compatibility matrix $(n_\varepsilon, n_{ldof})$, $\mathbf{N}_\lambda$ and $\mathbf{N}_\mathrm{d}$ are the plastic multiplier and phase-field shape function vectors $(1, n_{en})$, and $\mathbf{B}_\lambda$ and $\mathbf{B}_\mathrm{d}$ are plastic multiplier and phase-field gradient matrices (n_{dim}, n_{en}). The global assembly is formally performed with the boolean connectivity matrices $\mathbf{C}_{e,\mathrm{u}}$ (n_{ldof}, n_{dof}), $\mathbf{C}_{e,\lambda}$ (n_{en}, n_{np}), and $\mathbf{C}_{e,\mathrm{d}}$ (n_{en}, n_{np}) such that:

$$\hat{\mathbf{u}}_e = \mathbf{C}_{e,\mathrm{u}}\, \hat{\mathbf{u}} \quad , \quad \hat{\boldsymbol{\lambda}}_e = \mathbf{C}_{e,\lambda}\, \hat{\boldsymbol{\lambda}} \quad , \quad \hat{\mathbf{d}}_e = \mathbf{C}_{e,\mathrm{d}}\, \hat{\mathbf{d}} \tag{47}$$

4.1. Balance equations

The weak form of the equilibrium equation (22a) and of the plasticity $(26)_c$ and fracture $(30)_c$ complementarity equations are spatially discretized:

$$\delta\hat{\mathbf{u}}^\mathrm{T} \left[\sum_{e=1}^{n_{el}} \mathbf{C}_{e,\mathrm{u}}^\mathrm{T} \left(\int_{\Omega_{0e}} \mathbf{B}_\mathrm{u}^\mathrm{T} \boldsymbol{\sigma}\, \mathrm{d}\Omega_{0e} - \int_{\Omega_{0e}} \mathbf{N}_\mathrm{u}^\mathrm{T}\, \mathbf{b}\, \mathrm{d}\Omega_{0e} - \int_{\partial\Omega_{0e}} \mathbf{N}_\mathrm{u}^\mathrm{T}\, \mathbf{t}\, \mathrm{d}\Gamma_e \right) \right] = 0 \tag{48}$$

$$\Delta\hat{\boldsymbol{\lambda}}^\mathrm{T} \left[\sum_{e=1}^{n_{el}} \mathbf{C}_{e,\lambda}^\mathrm{T} \left(\int_{\Omega_{0e}} \omega \left[-\mathbf{N}_\lambda^\mathrm{T} f_y + c_p\, \mathbf{B}_\lambda^\mathrm{T}\, \boldsymbol{\nabla}\lambda \right] \mathrm{d}\Omega_{0e} \right) \right] = 0 \tag{49}$$

$$\Delta\hat{\mathbf{d}}^\mathrm{T} \left[\sum_{e=1}^{n_{el}} \mathbf{C}_{e,\mathrm{d}}^\mathrm{T} \left(\int_{\Omega_{0e}} \left\{ \mathbf{N}_\mathrm{d}^\mathrm{T} \left[\omega'\, \tilde{\psi}_0 + (f+1)\, w' + \frac{\eta_f}{\Delta t}\, \Delta d \right] + c_d\, \mathbf{B}_\mathrm{d}^\mathrm{T}\, \boldsymbol{\nabla}d \right\} \mathrm{d}\Omega_{0e} \right) \right] = 0 \tag{50}$$

where e denotes the element number and n_{el} is the total number of elements in the mesh. The stress tensor in Voigt notation $\boldsymbol{\sigma}$ is a vector with dimension $(n_\sigma, 1)$, being $n_\sigma = n_\varepsilon$ the number of independent stress components. The element integrals are evaluated over the element nominal volume Ω_{0e}. The element internal force vector $\mathbf{F}_{\mathrm{I},e}$ $(n_{ldof}, 1)$, the external force vector $\mathbf{F}_{\mathrm{E},e}$ $(n_{ldof}, 1)$, the yield vector $\mathbf{f}_{\mathrm{Y},e}$ $(n_{en}, 1)$, and the fracture activation vector $\mathbf{f}_{\mathrm{D},e}$ $(n_{en}, 1)$ are defined as:

$$\mathbf{F}_{\mathrm{I},e} := \int_{\Omega_{0e}} \mathbf{B}_{\mathrm{u}}^{\mathrm{T}} \left(\omega\, \boldsymbol{\sigma}_0^A + \boldsymbol{\sigma}_0^I \right) \mathrm{d}\Omega_{0e} \tag{51a}$$

$$\mathbf{F}_{\mathrm{E},e} := \int_{\Omega_{0e}} \mathbf{N}_{\mathrm{u}}^{\mathrm{T}}\, \mathbf{b}\, \mathrm{d}\Omega_{0e} + \int_{\partial\Omega_{0e}} \mathbf{N}_{\mathrm{u}}^{\mathrm{T}}\, \mathbf{t}\, \mathrm{d}\Gamma_{0e} \tag{51b}$$

$$\mathbf{f}_{\mathrm{Y},e} := \int_{\Omega_{0e}} \omega \left(\mathbf{N}_{\lambda}^{\mathrm{T}} f_y - c_p\, \mathbf{B}_{\lambda}^{\mathrm{T}}\, \nabla\lambda \right) \mathrm{d}\Omega_{0e} \tag{51c}$$

$$\mathbf{f}_{\mathrm{D},e} := -\int_{\Omega_{0e}} \left\{ \mathbf{N}_{\mathrm{d}}^{\mathrm{T}} \left[\omega'\, \tilde{\psi}_0 + (f+1)\, w' + w'_\epsilon + \frac{\eta_f}{\Delta t}\, \Delta d \right] + c_d\, \mathbf{B}_{\mathrm{d}}^{\mathrm{T}}\, \nabla d \right\} \mathrm{d}\Omega_{0e} \tag{51d}$$

where $\boldsymbol{\sigma}_0^A$, $\boldsymbol{\sigma}_0^I$ are defined in (36) and $\nabla\lambda$, Δd and ∇d are discretized as in (46). The additional constant term w'_ϵ is introduced to avoid spurious damage activations when $\alpha < \alpha_{cr}$ and is defined as:

$$w'_\epsilon = \epsilon\, \frac{G_c}{l_{0d}}\, \mathrm{H}^- (\alpha - \alpha_{cr}) \tag{52}$$

where ϵ is non-dimensional, small coefficient to be set as small as possible (usually taken equal to 10^{-2}), and $\mathrm{H}^-(\cdot)$ is the negative Heaviside operator. The spatial discretization of the governing equations reads:

$$\mathbf{F}_{\mathrm{I}} - \mathbf{F}_{\mathrm{E}} = \mathbf{0} \tag{53a}$$

$$\Delta\hat{\boldsymbol{\lambda}} \geq \mathbf{0} \quad , \quad \mathbf{f}_{\mathrm{Y}} \leq \mathbf{0} \quad , \quad \Delta\hat{\boldsymbol{\lambda}}^{\mathrm{T}}\, \mathbf{f}_{\mathrm{Y}} = 0 \tag{53b}$$

$$\Delta\hat{\mathbf{d}} \geq \mathbf{0} \quad , \quad \mathbf{f}_{\mathrm{D}} \leq \mathbf{0} \quad , \quad \Delta\hat{\mathbf{d}}^{\mathrm{T}}\, \mathbf{f}_{\mathrm{D}} = 0 \tag{53c}$$

5. Algorithmic implementation

5.1. Staggered scheme

The algorithmic solution of the set of governing equations (53) relies on the alternate minimization scheme illustrated in Algorithm 1. At each time step from t^n to t^{n+1}, the input is the solution at the previous step $(\hat{\mathbf{u}}, \hat{\boldsymbol{\lambda}}, \hat{\mathbf{d}})_n$, the increment of displacement Dirichelet boundary conditions $\Delta\hat{\mathbf{u}}_{\mathrm{D}}$ and the increment of external forces $\Delta\mathbf{F}_{\mathrm{E}}$. The staggered scheme is solved with an iterative procedure, where i denotes the staggered iteration counter. First, the elastoplastic problem (53a) and (53b) in $\hat{\mathbf{u}}$ and $\Delta\hat{\boldsymbol{\lambda}}$ is solved in a monolithic fashion with a Newton-Raphson scheme, for fixed phase-field $\Delta\hat{\mathbf{d}}_{i-1}$. The residuum of this inner monolithic loop, with iteration counter k, is a suitable measure of the out-of-balance forces $\mathbf{F}_{\mathrm{I}} - \mathbf{F}_{\mathrm{E}}$ and is denoted with $\texttt{res}_M$. The corresponding tolerance is $\texttt{TOL}_M$, where the M subscript stands for monolithic. Then, the elastoplastic solution $(\hat{\mathbf{u}}, \hat{\boldsymbol{\lambda}})_k$ is used to solve the phase-field activation criterion for frozen displacement and plastic multiplier. Finally, the residual $\texttt{res}_{STAG}$ of the staggered scheme is computed. It measures again the out-of-balance forces, but with the updated damage. The complementarity problems (53b) and (53c) are solved using the Mangasarian [33] Projected Successive Over-Relaxation algorithm (PSOR), following the approach proposed in [34]. Further details are given in Appendix C.

Algorithm 1: Alternate minimization scheme

input $(\hat{\mathbf{u}}, \hat{\boldsymbol{\lambda}}, \hat{\mathbf{d}})_n$, $\Delta\hat{\mathbf{u}}_{\mathrm{D}}$, $\Delta\mathbf{F}_{\mathrm{E}}$

initialize $(\hat{\mathbf{u}}, \hat{\boldsymbol{\lambda}}, \hat{\mathbf{d}})_i = (\hat{\mathbf{u}}, \hat{\boldsymbol{\lambda}}, \hat{\mathbf{d}})_n$

while ($\mathit{res}_{STAG} > \mathit{TOL}_{STAG}$) **do**

update $i = i + 1$

while ($\mathit{res}_M > \mathit{TOL}_M$) **do**

update $k = k + 1$

set $\mathbf{F}_{\mathrm{I},k} = \mathbf{F}_{\mathrm{I}}(\Delta\hat{\mathbf{u}}_k, \Delta\hat{\boldsymbol{\lambda}}_k, \Delta\hat{\mathbf{d}}_{i-1}) \quad , \quad \mathbf{f}_{\mathrm{Y},k} = \mathbf{f}_{\mathrm{Y}}(\Delta\hat{\mathbf{u}}_k, \Delta\hat{\boldsymbol{\lambda}}_k, \Delta\hat{\mathbf{d}}_{i-1})$

solve $\begin{matrix} \mathbf{F}_{\mathrm{I},k} - \mathbf{F}_{\mathrm{E}} = \mathbf{0} \\ \Delta\hat{\boldsymbol{\lambda}}_k \geq \mathbf{0} \quad , \quad \mathbf{f}_{\mathrm{Y},k} \leq \mathbf{0} \quad , \quad \Delta\hat{\boldsymbol{\lambda}}_k^{\mathrm{T}} \, \mathbf{f}_{\mathrm{Y},k} = 0 \end{matrix} \quad \rightarrow \ (\Delta\hat{\mathbf{u}}_k, \Delta\hat{\boldsymbol{\lambda}}_k)$

assemble $\mathbf{R}_{\mathrm{u},k} = \mathbf{F}_{\mathrm{I},k}(\Delta\hat{\mathbf{u}}_k, \Delta\hat{\boldsymbol{\lambda}}_k, \Delta\hat{\mathbf{d}}_{i-1}) - \mathbf{F}_{\mathrm{E}}$

compute $\mathtt{res}_M = \mathbf{R}_{\mathrm{u},k}^{\mathrm{T}} \, \mathbf{R}_{\mathrm{u},k}$

end

set $(\hat{\mathbf{u}}, \hat{\boldsymbol{\lambda}})_i = (\hat{\mathbf{u}}, \hat{\boldsymbol{\lambda}})_k \quad , \quad \mathbf{f}_{\mathrm{D},i} = \mathbf{f}_{\mathrm{D}}(\Delta\hat{\mathbf{u}}_i, \Delta\hat{\boldsymbol{\lambda}}_i, \Delta\hat{\mathbf{d}})$

solve $\Delta\hat{\mathbf{d}} \geq \mathbf{0} \quad , \quad \mathbf{f}_{\mathrm{D},i} \leq \mathbf{0} \quad , \quad \Delta\hat{\mathbf{d}}^{\mathrm{T}} \, \mathbf{f}_{\mathrm{D},i} = 0 \quad \rightarrow \ \Delta\hat{\mathbf{d}}_i = \Delta\hat{\mathbf{d}}$

assemble $\mathbf{R}_{\mathrm{u},i} = \mathbf{F}_{\mathrm{I}}(\Delta\hat{\mathbf{u}}_i, \Delta\hat{\boldsymbol{\lambda}}_i, \Delta\hat{\mathbf{d}}_i) - \mathbf{F}_{\mathrm{E}}$

compute $\mathtt{res}_{STAG} = \mathbf{R}_{\mathrm{u},i}^{T} \, \mathbf{R}_{\mathrm{u},i}$

end

output $(\hat{\mathbf{u}}, \hat{\boldsymbol{\lambda}}, \hat{\mathbf{d}})_n = (\hat{\mathbf{u}}, \hat{\boldsymbol{\lambda}}, \hat{\mathbf{d}})_i$

5.2. Monolithic elastoplastic solver

The solution scheme of the elastoplastic problem (53a) and (53b) is further detailed in this section. Since in the light of the staggered scheme this problem must be solved for fixed phase-field, the explicit dependence on the damage variable is omitted for the sake of clarity. The displacement residual vector $\mathbf{R}_{\mathrm{u}}$ (the iteration conter k has been omitted for notation convenience) has dimensions $(n_{dof}, 1)$ and measures the out-of-balance forces in the equilibrium equations:

$$\mathbf{R}_\mathrm{u}(\Delta\hat{\mathbf{u}}, \Delta\hat{\boldsymbol{\lambda}}) := \mathbf{F}_\mathrm{I}(\Delta\hat{\mathbf{u}}, \Delta\hat{\boldsymbol{\lambda}}) - \mathbf{F}_\mathrm{E} \tag{54}$$

The solution of the balance of linear momentum must fulfill the elastoplastic laws (53b). In practical terms, the loading-unloading conditions (53b) must be solved for fixed displacement increment, with the additional difficulty that, due to the presence of the gradient term, the elastoplastic return mapping algorithm has to be formulated as a global problem and the time integration of the constitutive law cannot be carried out element by element. Once a first estimate of the nodal plastic multiplier increment $\Delta\hat{\boldsymbol{\lambda}}$ is obtained, the set of active nodes $\mathcal{A}$ can be determined using the global PSOR algorithm:

$$\mathcal{A} := \left\{ a \in [1, n_{np}] \;\middle|\; \Delta\hat{\lambda}_a > 0 \right\} \tag{55}$$

where a is the global node label. The vanishing of the residuum $\mathbf{R}_\mathrm{u}$ is enforced by means of a Newton-Raphson iterative scheme. The estimate of the displacement increment update $\delta\Delta\hat{\mathbf{u}}$ between two successive iteration $k-1$ and k can be computed from the following conditions, resulting from the linearization of $\mathbf{R}_\mathrm{u}$ and $\mathbf{f}_\mathrm{Y}$ around the current solution $\hat{\mathbf{u}}_{k-1}$, $\Delta\hat{\boldsymbol{\lambda}}_{k-1}$:

$$\delta\mathbf{R}_\mathrm{u} + \mathbf{R}_\mathrm{u} = \mathbf{0} \quad , \quad \delta\mathbf{f}_\mathrm{Y}\big|_{\mathcal{A}} = \mathbf{0} \tag{56}$$

where $(\cdot)|_{\mathcal{A}}$ is the restriction over the set of active nodes. The linearizations read:

$$\delta\mathbf{R}_\mathrm{u} = \frac{\partial\mathbf{R}_\mathrm{u}}{\partial\hat{\mathbf{u}}}\,\delta\Delta\hat{\mathbf{u}} \quad + \left.\frac{\partial\mathbf{R}_\mathrm{u}}{\partial\hat{\boldsymbol{\lambda}}}\right|_{\mathcal{A}} \delta\Delta\hat{\boldsymbol{\lambda}}\big|_{\mathcal{A}} = \mathbf{K}_\mathrm{uu}\,\delta\Delta\hat{\mathbf{u}} + \mathbf{K}_{\mathrm{u}\lambda}\big|_{\mathcal{A}}\,\delta\Delta\hat{\boldsymbol{\lambda}}\big|_{\mathcal{A}} \tag{57a}$$

$$\delta\mathbf{f}_\mathrm{Y} = \left.\frac{\partial\mathbf{f}_\mathrm{Y}}{\partial\hat{\mathbf{u}}}\right|_{\mathcal{A}} \delta\Delta\hat{\mathbf{u}} + \left.\frac{\partial\mathbf{f}_\mathrm{Y}}{\partial\hat{\boldsymbol{\lambda}}}\right|_{\mathcal{A}} \delta\Delta\hat{\boldsymbol{\lambda}}\big|_{\mathcal{A}} = \mathbf{K}_{\lambda\mathrm{u}}\,\delta\Delta\hat{\mathbf{u}} + \mathbf{K}_{\lambda\lambda}\big|_{\mathcal{A}}\,\delta\Delta\hat{\boldsymbol{\lambda}}\big|_{\mathcal{A}} \tag{57b}$$

Therefore, the solving system becomes:

$$\begin{bmatrix} \mathbf{K}_\mathrm{uu} & \mathbf{K}_{\mathrm{u}\lambda}\big|_{\mathcal{A}} \\ \mathbf{K}_{\lambda\mathrm{u}}\big|_{\mathcal{A}} & \mathbf{K}_{\lambda\lambda}\big|_{\mathcal{A}} \end{bmatrix}_{k-1} \begin{vmatrix} \delta\Delta\hat{\mathbf{u}} \\ \delta\Delta\hat{\boldsymbol{\lambda}}\big|_{\mathcal{A}} \end{vmatrix} = - \begin{vmatrix} \mathbf{R}_\mathrm{u} \\ \mathbf{0} \end{vmatrix}_{k-1} \tag{58}$$

It is important to remark that this system is needed only to recover the correct algorithmic tangent stiffness for the estimation of the displacement update $\delta\Delta\hat{\mathbf{u}}$ through (57a). Once the system has been solved for $\delta\Delta\hat{\mathbf{u}}$, the value of the update $\delta\Delta\hat{\boldsymbol{\lambda}}\big|_{\mathcal{A}}$ is not used in the current algorithm. As shown in Algorithm 2, it is evident how the adopted procedure resembles a classical Newton-Raphson scheme for local plasticity, but with the introduction of a global return mapping. The explicit expressions of the tangent matrix and residuals are provided in Appendix A. When large time steps are used, convergence may become difficult. especially when damage is activated. To overcome convergence problems, a line search procedure has been used as outlined in Appendix B.

Algorithm 2: Monolithic elastoplastic solver

while ($res_M > TOL_M$) **do**

assemble $\mathbf{K}_{uu}(\Delta\hat{\mathbf{u}}_k, \Delta\hat{\boldsymbol{\lambda}}_k)$, $\mathbf{K}_{u\lambda}(\Delta\hat{\mathbf{u}}_k)$, $\mathbf{K}_{\lambda\lambda}$

update $k = k + 1$

solve $\begin{bmatrix} \mathbf{K}_{uu} & \mathbf{K}_{u\lambda}\big|_{\mathcal{A}} \\ \mathbf{K}_{\lambda u}\big|_{\mathcal{A}} & \mathbf{K}_{\lambda\lambda}\big|_{\mathcal{A}} \end{bmatrix}_{k-1} \begin{vmatrix} \delta\Delta\hat{\mathbf{u}} \\ \delta\Delta\hat{\boldsymbol{\lambda}}\big|_{\mathcal{A}} \end{vmatrix} = - \begin{vmatrix} \mathbf{R}_u \\ \mathbf{0} \end{vmatrix}_{k-1} \quad \rightarrow \Delta\hat{\mathbf{u}}_k = \Delta\hat{\mathbf{u}}_{k-1} + \delta\Delta\hat{\mathbf{u}}$

set $\mathbf{f}_{Y,k} = \mathbf{f}_Y(\Delta\hat{\mathbf{u}}_k, \Delta\hat{\boldsymbol{\lambda}})$

solve $\Delta\hat{\boldsymbol{\lambda}} \geq \mathbf{0} \quad , \quad \mathbf{f}_{Y,k} \leq \mathbf{0} \quad , \quad \Delta\hat{\boldsymbol{\lambda}}^{\mathrm{T}}\, \mathbf{f}_{Y,k} = 0 \quad \rightarrow \Delta\hat{\boldsymbol{\lambda}}_k = \Delta\hat{\boldsymbol{\lambda}}$

define $\mathcal{A} := \{ \, a \in [1, n_{np}] \mid \Delta\hat{\lambda}_{k,a} > 0 \, \}$

assemble $\mathbf{R}_{u,k}(\Delta\hat{\mathbf{u}}_k, \Delta\hat{\boldsymbol{\lambda}}_k)$

compute $\mathtt{res}_M = \mathbf{R}^T_{u,k}\, \mathbf{R}_{u,k}$

end

6. Numerical simulations

Two-dimensional simulations are performed with 4-nodes quadrilateral elements in plane strain conditions. One of the consequences of the effective stress approach is that plastic strains continue to develop until the final stage of failure, therefore requiring a suitable treatment of plastic locking. Here, a reduced one-point integration rule with hourglass control has been used for all fields $\mathbf{u}, \lambda, d$, in line with what proposed in [47]. The staggered residual tolerance is $\mathtt{TOL}_{STAG} = 10^{-3}\,\mathrm{N}^2$, while the monolithic Newton-Raphson residual tolerance is $\mathtt{TOL}_M = 10^{-6}\,\mathrm{N}^2$. The mesh resolution of the phase-field localization band is reported for each test comparing the element dimension h_e and the damage internal length parameter l_{0d}, which for the AT1 dissipation model represents a fourth of the band width (see e.g. [48]).

Material	E_0	ν	K_0	G_0	σ_0	H_0	l_{0p}	G_c
I	68.90	0.33	-	-	465	10	1.2	10
II	-	-	71.66	27.28	340	250	1.6	9.31
	GPa	-	GPa	GPa	MPa	MPa	mm	N/mm

Table 1: Material properties

6.1. One-dimensional localization

The tensile loading of a one-dimensional bar is considered. The geometry and boundary conditions are depicted in Figure 4. The cross section is assumed to be $A = 1\,mm^2$. The material properties are $E_0 = 210\,GPa$, $\sigma_0 = 350\,MPa$, $H_0 = 650\,MPa$, $l_{0p} = 0.06\,mm$, and $G_c = 2\,N/mm$. The fracture internal length is $l_{0d} = 0.03\,mm$. The ductile fracture parameters are $\alpha_{cr} = 0.4$, $\Delta\alpha_{cr} = 0.2$ and $f_{min} = 0$. The viscous coefficient $\bar{\eta} = 5 \cdot 10^{-3}\,s$.

A uniform mesh of 500 linear one-dimensional finite elements is used with an element size $h_e = 0.002\,mm$. A uniform time discretization is used to enforce the boundary conditions. The total number of steps is $n_{st} = 1000$ and the step increment is $\Delta\bar{u} = 5 \cdot 10^{-4}\,mm$. The localization in the central part of the bar is obtained with a local weakening of the material properties in the central 10% of its length. In these elements, the yield stress σ_0 and the toughness G_c are reduced by 20%. For this particular 1D example, the staggered residual tolerance is $\texttt{TOL}_{STAG} = 10^{-5}\,\mathrm{N}^2$, while the monolithic Newton-Raphson residual tolerance is $\texttt{TOL}_M = 10^{-10}\,\mathrm{N}^2$.

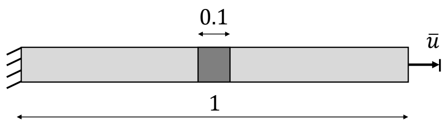

Figure 4: One-dimensional bar in tension: geometry [mm] and boundary conditions.

The global response in terms of engineering strain and stress is shown in Figure 5a. Here, some significant steps are highlighted with circular markers. The corresponding profiles of the modulation function $f + 1$ are then plotted in Figure 5b. The first time at which a point reaches $\alpha = \alpha_{cr}$ is step 680. The competition between the terms $(1 - \bar{d})$ and $\tilde{\mathcal{H}}$ starts at step 737. Until that moment, the qualitative profile of the modulation function resembles the one of the equivalent plastic deformation. After that, the points experiencing a plastic deformation $\alpha > \alpha_{cr}$ show a decrease in the value of $f + 1$, since the influence of the fictitious phase-field history $\bar{d}$ significantly intervenes into the modulation function.

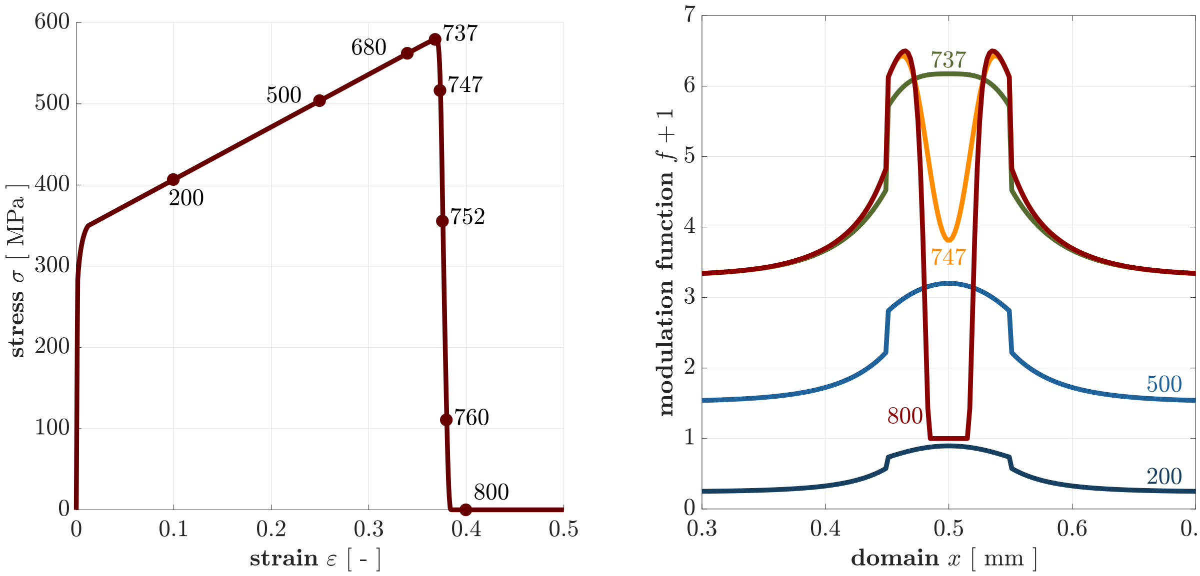

(a) Engineering stress vs strain curve

(b) Modulation function evolution

Figure 5: 1D localization. Global response (a) and modulation function time evolution (different colors correspond to different times) (b).

The time and space evolution of the equivalent plastic deformation and of the phase field can be observed in Figure 6. The circular markers correspond to the mesh nodes. Before damage onset, only the plastic deformation profile is different from zero as shown in the plot of step 680, when for the first time $\alpha = \alpha_{cr}$ is reached. Here, the uniform solution of the equivalent plastic deformation is slightly perturbed by the weakening of the material parameters. In the following steps, the damage localization induces a more intense localization of plastic deformations, due to the effective stress approach adopted in the current work, with the material continuing to yield after damage development. Since the effective stress is acting on the continuous part of the material bulk and this is progressively reducing, the plastic deformation increases considerably and, at this point, the effect of the gradient on the plastic multiplier can be appreciated because of the softening structural response. In the subsequent snapshots, it can be noticed how the damage growth is driven by the developing plastic strain. At step 752, the plastic deformation reaches $\alpha_{cr} + \Delta\alpha_{cr}$ for the first time. At step 800, the profiles of the equivalent plastic deformation and of the phase field are fully developed. The plasticity driven nature of fracture can be appreciated by noticing that the finite band-width of damage is entirely contained in the plastic localization band, since no damage occurs in the portion of the domain where $\alpha < \alpha_{cr}$.

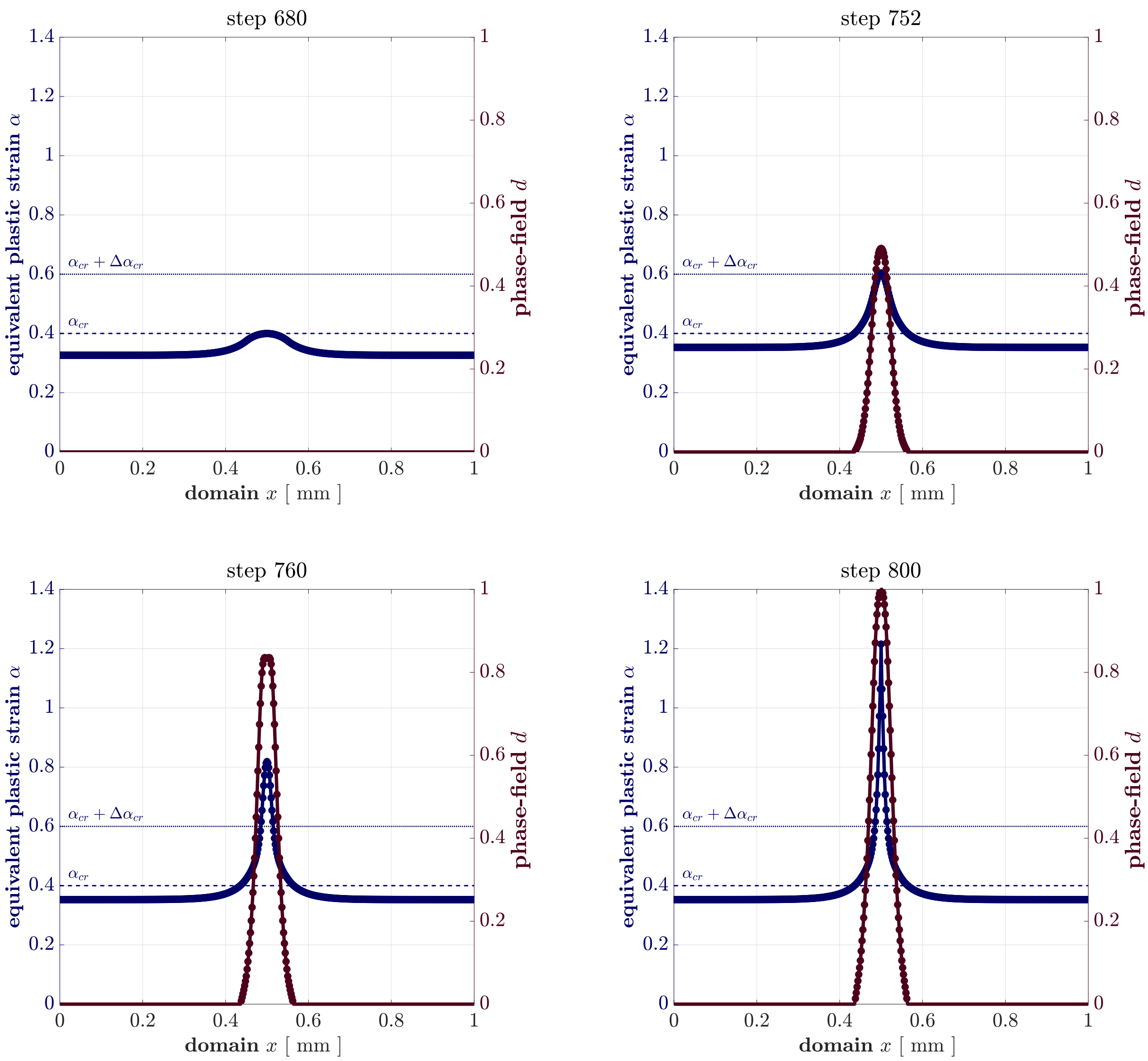

Figure 6: 1D localization. Equivalent plastic strain (blue curve) and phase-field time evolution (brown curve).

6.2. V-notched specimen

We consider the V-notched specimen experimentally tested in [49]. Several authors have used this benchmark for the simulation of ductile fracture (see, e.g., [19]). This is shown as a first example to demonstrate the model capabilities when crack onset and specimen failure occur without a stable propagation branch. The geometry of the specimen is depicted in Figure 7a. As in [49, 19], slightly rounded corners have been used at the notch tips to avoid sharp discontinuities in the geometry. The Dirichelet boundary conditions constrain the horizontal direction only. The material properties are shown in Table 1 for the

469 case of Material I. The phase-field internal length is $l_{0d} = 0.4\,mm$ and the ductile fracture parameters are
470 $\alpha_{cr} = 0.05$, $\Delta\alpha_{cr} = 0.03$ and $f_{min} = 0$.

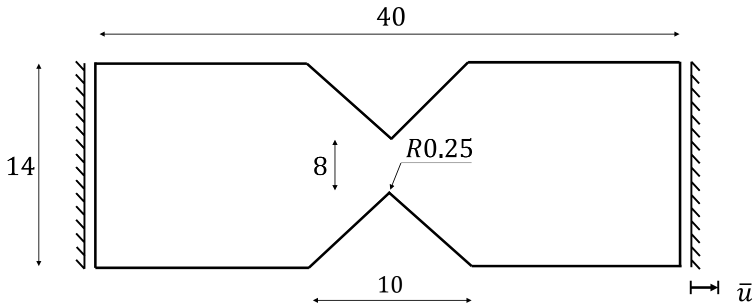

(a) Geometry in [mm] and boundary conditions

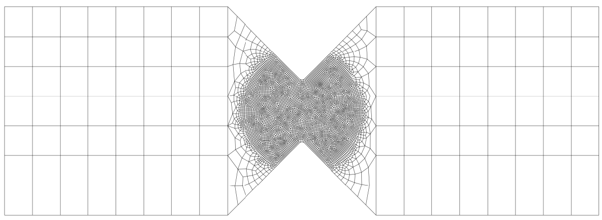

(b) Mesh

Figure 7: V-notched specimen. Geometry in [mm], boundary conditions and mesh.

471 The mesh is shown in Figure 7b. A refinement in the expected crack propagation region is used. The
472 minimum element side is $h_e = 0.1\,mm$. The resolution of the localization zone is $l_{0p}/h_e = 12$ for the plastic
473 deformation and $l_{0d}/h_e = 4$ for the phase field. A total of $n_{el} = 6359$ elements and $n_{np} = 6454$ nodes have
474 been used, with a time step $\Delta u = 0.01\,mm$.

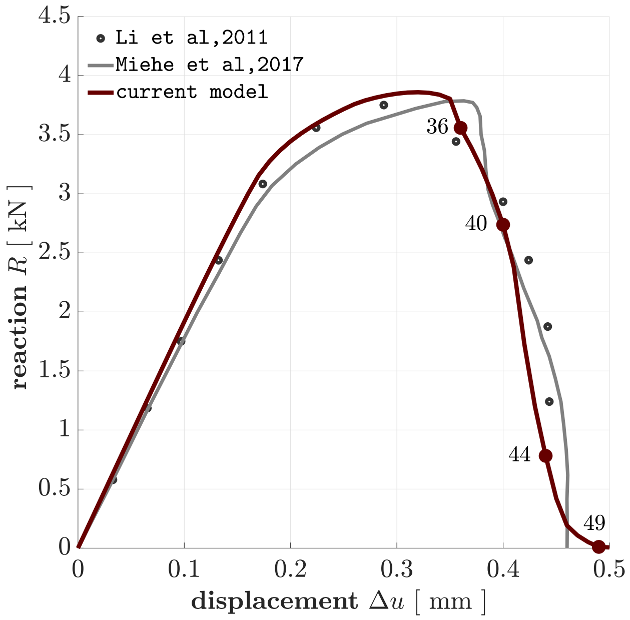

Figure 8: V-notched specimen. Reaction force vs imposed displacement. Results (solid black curve) are compared to those in [19] (light gray) and to the experimental results in [49] (circular markers).

The global response in terms of reaction force and enforced displacement at the right edge is shown in Figure 8. The viscous coefficient is set to a non-negligible value $\bar{\eta} = 0.08\,s$, to prevent overly brittle crack propagation. The response is purely elastoplastic until a displacement of $0.25\,mm$, corresponding to step 25, is enforced. Then, damage grows at both the notch tips until crack onset occurs between step 35 and 36. The two cracks propagate with an almost linear path until step 42, when the first crack starts to branch as it can be clearly noticed in step 44. The final coalescence of the two fractures occurs at step 49. The contour plots of the plastic multiplier λ and of the phase field d at the relevant steps in the reaction curve are shown in Figure 9. It must be noticed that, due to the plasticity driven nature of the proposed ductile fracture model, the crack propagation closely follows the path of the plasticity localization band observable in the contour plots of λ.

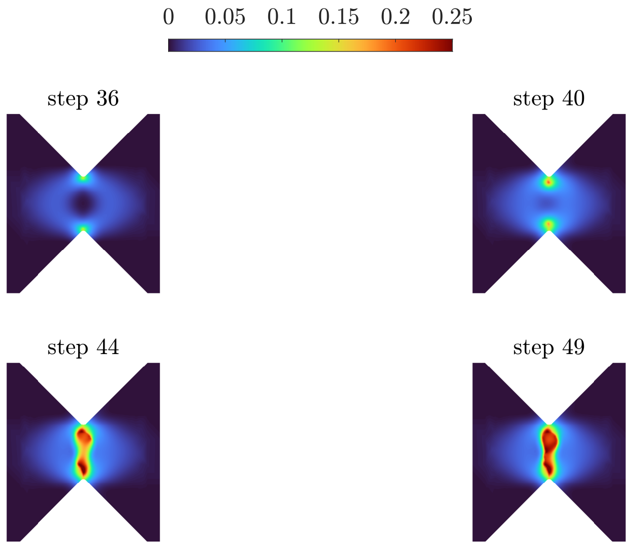

(a) Plastic multiplier λ

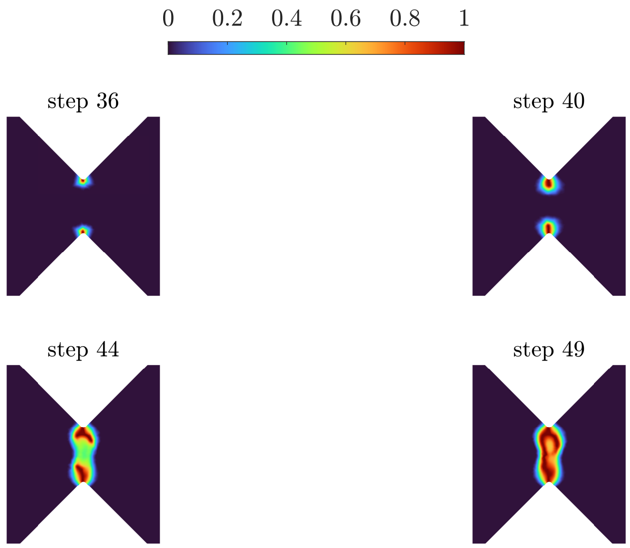

(b) Phase field d

Figure 9: V-notched specimen. Plastic multiplier and phase-field contourplots.

6.3. Symmetric notched specimen

This test has also been investigated by several authors, such as in [4] and [9]. In these two works, the ductile fracture simulation approach is significantly different from the current model. The main difference lies in the yield criterion being based on nominal stresses. When damage starts to propagate, nominal stresses decrease and the response of the damaged material becomes purely elastic, since the yield surface can be no more activated. This example is particularly interesting in view of the stable crack propagation that can be observed after damage reaches the unit value in the first notch. The geometry and boundary conditions are shown in Figure 10a. Both edges are clamped (i.e, no horizontal displacements are allowed) and the top boundary is subjected to an enforced vertical displacement. The uniform increment of Dirichelet boundary conditions at each step is $\Delta u = 0.01\,mm$.

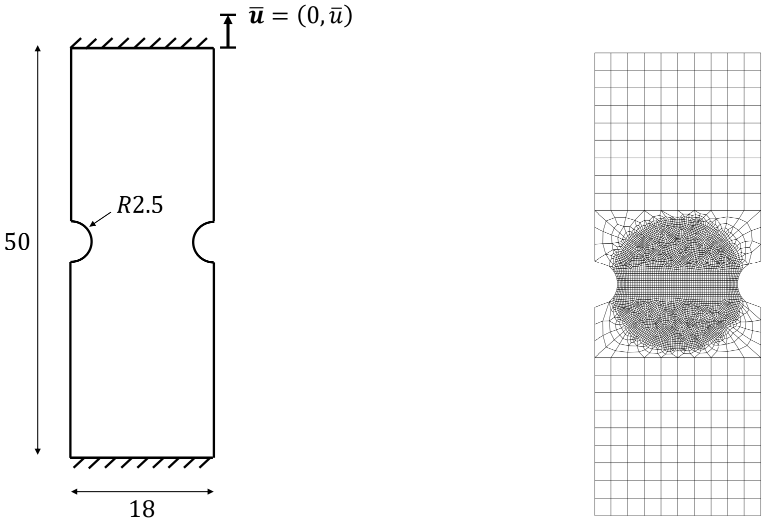

(a) Geometry in [mm] and boundary conditions

(b) Mesh

Figure 10: Symmetric notched specimen. Geometry in [mm], boundary conditions (a) and mesh (b).

The material properties are shown in Table 1 for the case of Material II. The phase-field internal length is $l_{0d} = 0.4\,mm$ and the ductile fracture parameters are $\alpha_{cr} = 0.09$, $\Delta\alpha_{cr} = 0.01$ and $f_{min} = 0$. The viscous coefficient is $\bar{\eta} = 0.01\,s$. The mesh for the simulation is shown in Figure 10b. A local refinement is introduced where the crack propagation is expected to occur. The minimum element side is $h_e = 0.2\,mm$. The resolution of the localization zone is $l_{0p}/h_e = 8$ for the plastic deformation and $l_{0d}/h_e = 2$ for the phase field. The number of elements is $n_{el} = 5438$ and the number of nodes is $n_{np} = 5494$.

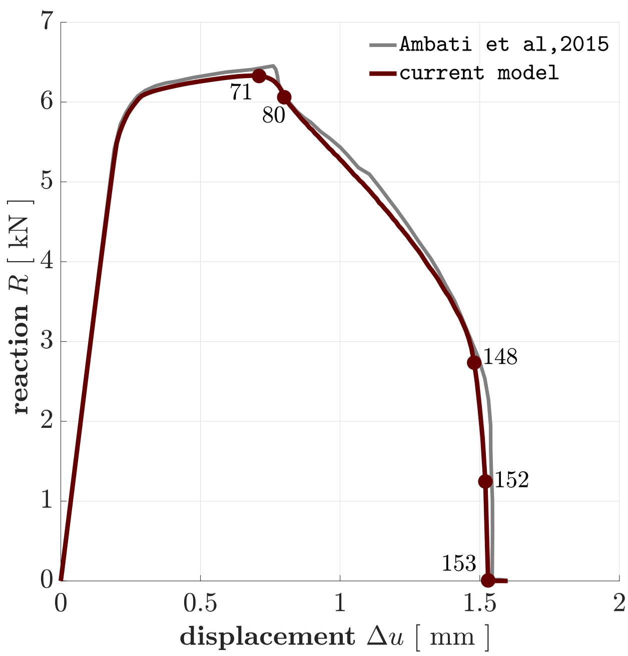

Figure 11: Symmetric notched specimen. Reaction force vs imposed displacement. Results are compared with those of the nominal stress approach proposed in Ambati et al [4].

The global response in terms of reaction force vs enforced vertical displacement at the top edge is depicted in Figure 11. The corresponding contour plots of plastic multiplier and phase field are shown in Figure 12. The response is purely elastoplastic until step 55 corresponding to $\bar{u} = 0.55\,mm$. In step 71 it is evident how shear bands form at an inclination of almost 45°. At step 80 ($\bar{u} = 0.80\,mm$), the right notch first reaches damage equal to unity. Afterwards, a long and stable horizontal crack propagation is observed from the right notch towards the opposite one. This mechanism continues until step 113 ($\bar{u} = 1.13\,mm$) with an almost linear softening slope. At this point the crack in the second notch appears. Then, in a few steps, a short stable propagation of this second crack is observed towards the opposite side. This mechanism is evident up to step 148 ($\bar{u} = 1.48\,mm$) when the cracks are so close that the merging of the two paths becomes possible. This sudden crack propagation ends with the specimen failure at step 153 ($\bar{u} = 1.53\,mm$).

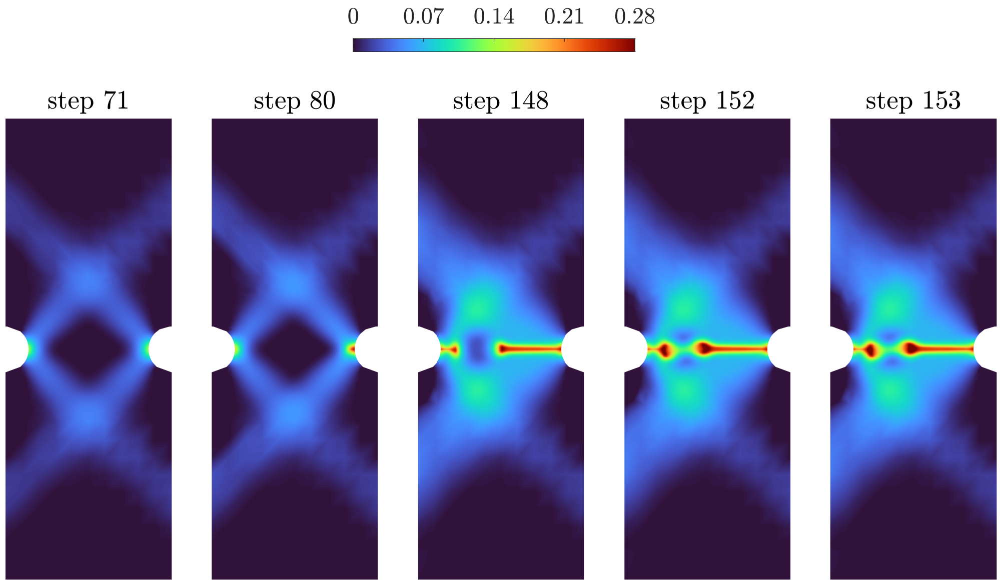

(a) Plastic multiplier λ

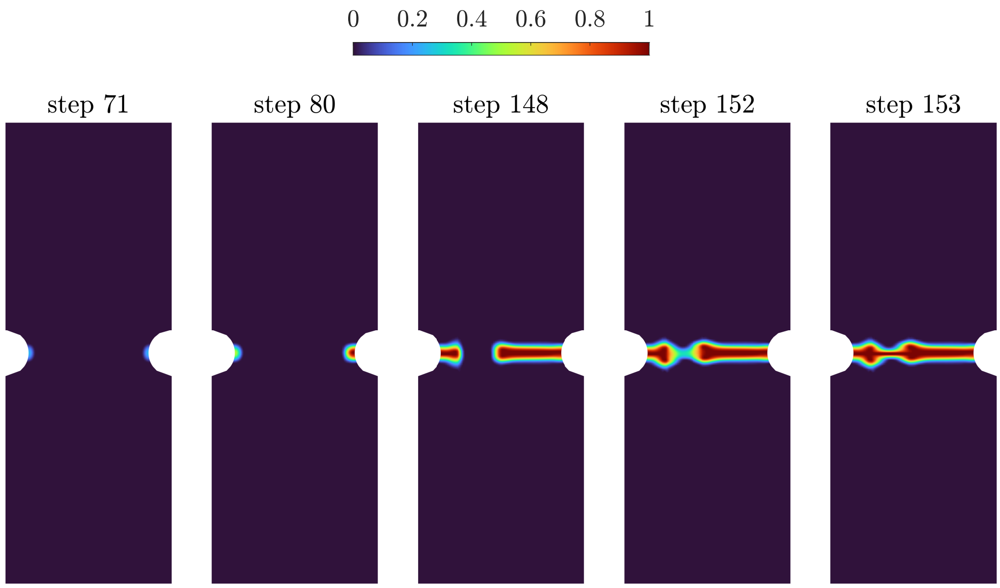

(b) Phase field d

Figure 12: Symmetric notched specimen. Plastic multiplier (a) and phase field (b) contour plots.

6.4. Asymmetric notched specimen

The asymmetric notched specimen with the geometry and boundary conditions depicted in Fig. 13a is considered. The bottom edge is fully clamped, while the top edge has fully constrained horizontal displacement, with an enforced vertical displacement $\bar{u}$. The material properties correspond to Material I in Table 1. The phase-field internal length is $l_{0d} = 0.6\,mm$ and the ductile fracture parameters are $\alpha_{cr} = 0.086$, $\Delta\alpha_{cr} = 0.05$ and $f_{min} = 0$. The viscous coefficient is $\bar{\eta} = 0.001\ s$.

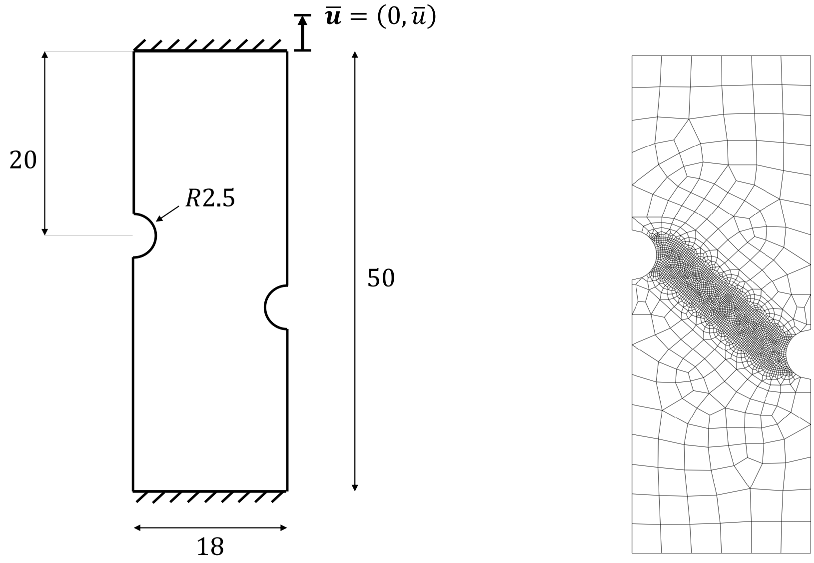

(a) Geometry in [mm] and boundary conditions

(b) Mesh

Figure 13: Asymmetric notched specimen. Geometry in [mm], boundary conditions (a) and mesh (b).

The mesh used is shown in Figure 13b. The spatial discretization is locally refined where the crack localization is expected to occur. The minimum element size is $h_e = 0.2\,mm$. Therefore, the resolution is $l_{0p}/h_e = 8$ and $l_{0d}/h_e = 3$. The number of elements is $n_{el} = 2637$ and the number of nodes is $n_{np} = 2686$. The time step is $\Delta u = 0.01\,mm$.

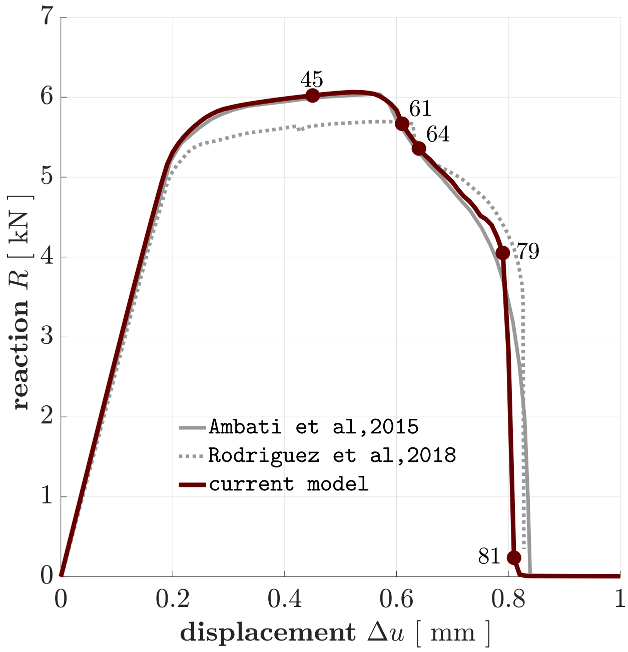

Figure 14: Asymmetric notched specimen. Reaction force vs imposed displacement. Results are compared with those obtained with the nominal stress approach proposed in Ambati et al [4] and the effective stress approach proposed in Rodriguez et al [11].

The global response in terms of reaction force and enforced displacement is shown in Figure 14. The structural response is elastoplastic until step 45 where a damage starts to develope at the upper notch. At step 61, the phase-field reaches unity for the first time. At step 64, fracture starts also from the lower notch. First, the cracks propagate horizontally from the two notches, then, in few steps, the two paths start to align along the shear band, i.e., in the direction of the driving plastic deformation. Finally, an unstable crack propagation occurs between steps 79 and 81, where the cracks merge.

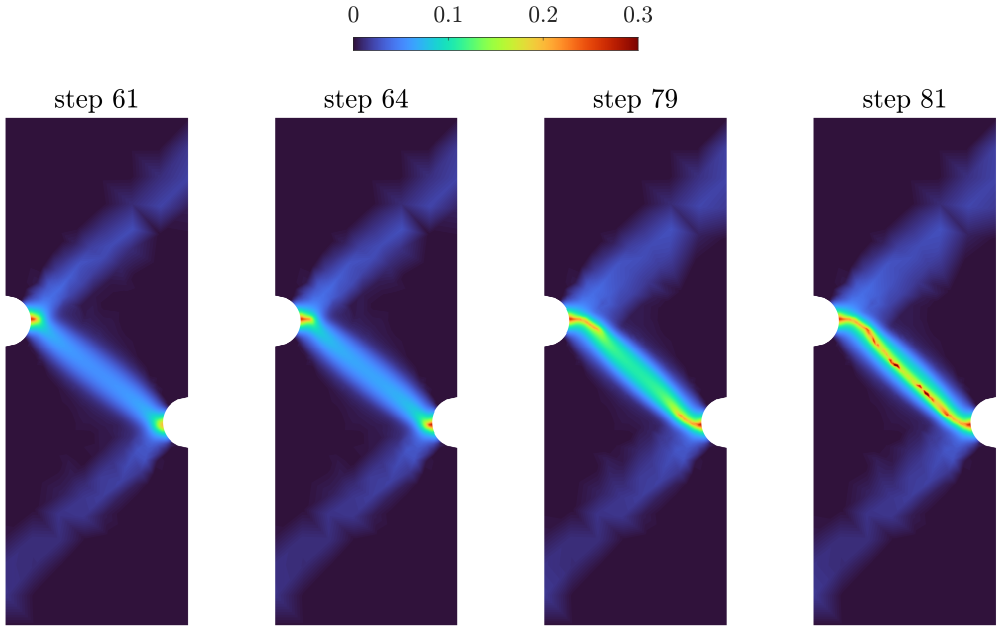

(a) Plastic multiplier λ

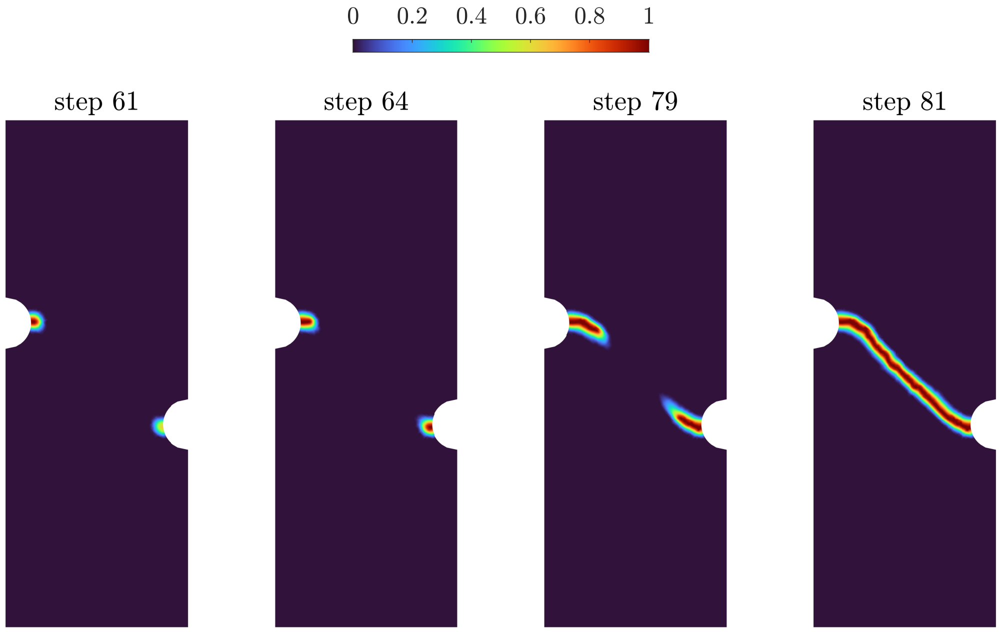

(b) Phase field d

Figure 15: Asymmetric notched specimen. Contour plots of plastic multiplier (a) and phase field (b).

7. Conclusions

A variational formulation of small strain ductile fracture, based on an AT1 phase-field modeling of crack propagation, has been proposed. The main features of the proposed model can be summarized as follows.

- A mixed variational statement has been formulated, incorporating a finite-step variational update for both gradient elastoplasticity and the phase field. The obtained functional is of a general form and can be used for any elastoplastic model belonging to the class of generalized standard materials [38].

- Irreversibility of both plastic and brittle dissipation has been enforced in a rigorous way formulating the two problems as global linear complementarity problems. Both problems have been solved using a very efficient explicit Projected Successive Over-Relaxation (PSOR) algorithm [33], following the approach proposed in [32, 34].

- The elastoplastic model has been formulated in terms of effective stresses, i.e. the true stresses acting on the non-damaged part of the bulk material. This has at least two important consequences. First, available implementations of elastoplastic models need not be modified and can be directly used as they are. This is of particular interest, e.g., in the case of anisotropic materials. Second, while in the case of nominal stresses plastic strains stop to grow as soon as damage starts to develop, in the case of effective stresses, plasticity continues to develop until the very final stage of rupture, making the gradient plasticity regularization necessary and also requiring a dedicated treatment of elastoplastic locking.

- In ductile fracture, damage growth is associated to locally high levels of plastic strains. A plasticity driven crack propagation model has therefore been formulated. The complex interaction between ductile and brittle dissipation has been modulated by the addition of a non-variational function of the equivalent plastic strain, in the line of what proposed by several other authors [4, 7, 9, 17]. The adopted modulation function depends on three parameters whose role is clearly identified and which can be easily determined based on a one-dimensional tension test. Another important feature, is that until a critical value of the equivalent plastic strain is achieved, the value of the modulation function is determined directly by the structural response and need not be established a priori, conferring great generality to its definition.

- A staggered algorithm has been formulated for the solution of the variational equations. The gradient elastoplastic problem is solved monolithically for fixed phase field, while the phase-field problem is solved for fixed displacements and plastic strains. The monolithic solution of the gradient elasto-plastic problem is often critical and requires special attention. A consistent global Newton-Raphson scheme has been formulated for the case of Mises plasticity, with a return mapping carried out at global level, together with a rigorous consistent tangent matrix. The convergence has been further improved supplementing the iterative scheme with a line-search procedure.

The proposed model has been applied to the simulation of several benchmark problems revealing excellent robustness, good accuracy and easy parameter identification. Extension to 3D finite strain ductile fracture is currently in progress.

Acknowledgements

Alessandro Marengo gratefully acknowledges the support by Innovhub and Tetra Pak Packaging Solutions. The support by the Italian Ministry of University and Research (MUR) through the PRIN project XFAST-SIMS (No. 20173C478N) is also gratefully acknowledged.

Appendix A. Linearizations for isotropic von-Mises gradient elastoplasticity

The linearizations needed for the solution of the gradient elastoplastic problem with the monolithic scheme in Algorithm 2 are developed below. All operations are perfomed for the gradient Mises elasto-plastic problem without damage and the zero subscript of the effective response is omitted for the sake of clarity. Voigt notation is used throughout this appendix. For instance, the stress vector is denoted with $\boldsymbol{\sigma}$. The linearization of the element internal forces vector reads:

$$
\begin{aligned}
\delta \mathbf{F}_{\mathrm{I},e} = \int_{\Omega_e} \mathbf{B}_{\mathrm{u}}^{\mathrm{T}} \, \delta\boldsymbol{\sigma} \, \mathrm{d}\Omega_e = & \underbrace{\left[\int_{\Omega_e} \mathbf{B}_{\mathrm{u}}^{\mathrm{T}} \left(\mathbf{D}^{el} - \Delta\lambda \, \mathbf{D}^{el}_{dev} \, \partial^2_{\boldsymbol{\sigma}\boldsymbol{\sigma}} f_y \, \mathbf{D}^{el}_{dev} \right) \mathbf{B}_{\mathrm{u}} \, \mathrm{d}\Omega_e \right]}_{\mathbf{K}_{\mathrm{uu},e}} \delta\hat{\mathbf{u}}_e + \\
& + \underbrace{\left[\int_{\Omega_e} \mathbf{B}_{\mathrm{u}}^{\mathrm{T}} \left(- \mathbf{D}^{el}_{dev} \, \partial_{\boldsymbol{\sigma}} f_y \right) \mathbf{N}_\lambda \, \mathrm{d}\Omega_e \right]}_{\mathbf{K}_{\mathrm{u}\lambda,e}} \delta\hat{\lambda}_e
\end{aligned}
\tag{A.1}
$$

where $\mathbf{D}^{el} = \partial^2_{\boldsymbol{\varepsilon}\boldsymbol{\varepsilon}} \psi^e$ is the matrix of elastic moduli and the deviatoric nature of the plastic deformation vector $\boldsymbol{\varepsilon}^p$ has been exploited. $\mathbf{D}^{el}_{dev}$ is the deviatoric elastic stiffness matrix. The linearization of the element yield vector reads:

$$\begin{aligned}\delta\mathbf{f}_{\mathrm{Y},e} &= \int_{\Omega_e}\left[\mathbf{N}_\lambda^{\mathrm{T}}\,\delta f_y - c_p\,\mathbf{B}_\lambda^{\mathrm{T}}\,\nabla\delta\lambda\right]\mathrm{d}\Omega_e = \\ &= \underbrace{\left[\int_{\Omega_e}\mathbf{N}_\lambda^{\mathrm{T}}\left(\mathbf{D}^{el}_{dev}\,\partial_{\boldsymbol{\sigma}} f_y\right)^{\mathrm{T}}\mathbf{B}_{\mathrm{u}}\,\mathrm{d}\Omega_e\right]}_{\mathbf{K}_{\lambda\mathrm{u},e}}\delta\hat{\mathbf{u}}_e + \\ &\quad \underbrace{-\left[\int_{\Omega_e}\left\{\mathbf{N}_\lambda^{\mathrm{T}}\left(\partial_{\boldsymbol{\sigma}} f_y^{\mathrm{T}}\,\mathbf{D}^{el}_{dev}\,\partial_{\boldsymbol{\sigma}} f_y + \partial_\lambda\chi\right)\mathbf{N}_\lambda + c_p\,\mathbf{B}_\lambda^{\mathrm{T}}\,\mathbf{B}_\lambda\right\}\mathrm{d}\Omega_e\right]}_{\mathbf{K}_{\lambda\lambda,e}}\delta\hat{\boldsymbol{\lambda}}_e\end{aligned} \tag{A.2}$$

The deviatoric elastic stiffness matrix for the isotropic case is $\mathbf{D}^{el}_{dev} = 2G\,\mathbf{I}_{dev}$, where $\mathbf{I}_{dev}$ is the deviatoric projection matrix. The use of von-Mises yield function with isotropic linear hardening leads to:

$$\Delta\lambda\,\mathbf{D}^{el}_{dev}\,\partial^2_{\boldsymbol{\sigma}\boldsymbol{\sigma}} f_y\,\mathbf{D}^{el}_{dev} = 2G\beta\left(\mathbf{I}_{dev} - \mathbf{n}^{tr}\,\mathbf{n}^{tr\mathrm{T}}\right)$$

$$\mathbf{D}^{el}_{dev}\,\partial_{\boldsymbol{\sigma}} f_y = 3G\,\frac{\mathbf{s}^{tr}}{\sigma^{tr}_{eq}} \quad , \quad \partial_{\boldsymbol{\sigma}} f_y^{\mathrm{T}}\,\mathbf{D}^{el}_{dev}\,\partial_{\boldsymbol{\sigma}} f_y = 3G$$

where $\mathbf{s}^{tr}$ is the trial elastic deviatoric stress vector, $\mathbf{n}^{tr} = \mathbf{s}^{tr}/|\mathbf{s}^{tr}|$ is the trial yield surface unit normal vector, $\sigma^{tr}_{eq} = \sqrt{3/2\,\mathsf{s}^{tr} : \mathsf{s}^{tr}}$ is the trial equivalent stress (being s the deviatoric stress tensor with Voigt notation $\mathbf{s}$), and $\beta := 3G\,\Delta\lambda/\sigma^{tr}_{eq}$. The element tangent stiffness matrices and the internal forces vector are:

$$\mathbf{K}_{\mathrm{uu},e} = \int_{\Omega_e}\mathbf{B}_{\mathrm{u}}^{\mathrm{T}}\left[\mathbf{D}^{el} - 2G\beta\left(\mathbf{I}_{dev} - \mathbf{n}^{tr}\,\mathbf{n}^{tr\mathrm{T}}\right)\right]\mathbf{B}_{\mathrm{u}}\,\mathrm{d}\Omega_e \tag{A.3a}$$

$$\mathbf{K}_{\mathrm{u}\lambda,e} = \int_{\Omega_e}\mathbf{B}_{\mathrm{u}}^{\mathrm{T}}\left(-3G\,\frac{\mathbf{s}^{tr}}{\sigma^{tr}_{eq}}\right)\mathbf{N}_\lambda\,\mathrm{d}\Omega_e = \mathbf{K}^{\mathrm{T}}_{\lambda\mathrm{u},e} \tag{A.3b}$$

$$\mathbf{K}_{\lambda\lambda,e} = -\int_{\Omega_e}\left[\left(3G + H\right)\mathbf{N}_\lambda^{\mathrm{T}}\,\mathbf{N}_\lambda + c_p\,\mathbf{B}_\lambda^{\mathrm{T}}\,\mathbf{B}_\lambda\right]\mathrm{d}\Omega_e \tag{A.3c}$$

$$\mathbf{F}_{\mathrm{I},e} = \int_{\Omega_e}\mathbf{B}_{\mathrm{u}}^{\mathrm{T}}\left[p\,\mathbf{1} + (1-\beta)\,\mathbf{s}^{tr}\right]\mathrm{d}\Omega_e \tag{A.3d}$$

where $\mathbf{1}$ is the spherical projection vector in Voigt notation.

Appendix B. Steepest descent or backtracking line search

The implemented line search procedure is based on what proposed in [50]. The global return mapping outlined in Section 5.2 for the elastoplastic gradient problem with fixed damage shows how the loading-unloading condition (53b) is a purely displacement driven problem. Therefore, without loss of generality, it can be stated that the total energy is a function of displacement only $\Pi_p^{\nabla\,n}(\Delta\hat{\mathbf{u}})$. The solution update $\delta\Delta\hat{\mathbf{u}}$

between two subsequent Newton iterations $k-1$ and k is the result of the monolithic system (58) and the current solution can be written as follows:

$$\Delta\hat{\mathbf{u}}_k = \Delta\hat{\mathbf{u}}_{k-1} + \delta\Delta\hat{\mathbf{u}} \tag{B.1}$$

The new solution estimate should satisfy the condition $\Pi_p^{\nabla\,n}(\Delta\hat{\mathbf{u}}_k) < \Pi_p^{\nabla\,n}(\Delta\hat{\mathbf{u}}_{k-1})$. Yet, this condition may not be always fullfiled by the Newton algorithm. Therefore, a line search procedure has been implemented. The step length parameter γ_k is defined such that:

$$\Delta\hat{\mathbf{u}}_k = \Delta\hat{\mathbf{u}}_{k-1} + \gamma_k\,\delta\Delta\hat{\mathbf{u}} \tag{B.2}$$

The optimal step length minimizes the total energy between the two iterations $k-1$ and k:

$$\gamma_k = \arg\min_{\gamma_k^*}\left[\Pi_p^{\nabla\,n}\left(\Delta\hat{\mathbf{u}}_{k-1} + \gamma_k^*\,\delta\Delta\hat{\mathbf{u}}_k\right)\right] \tag{B.3}$$

For non-quadratic objective functions $\Pi(\Delta\hat{\mathbf{u}})$ there is no closed form solution of the problem (B.3). Therefore, a standard procedure involves the satisfaction of the so-called Wolfe condition:

$$\Pi_p^{\nabla\,n}(\Delta\hat{\mathbf{u}}_{k-1} + \gamma_k\,\delta\Delta\hat{\mathbf{u}}_k) < \Pi_p^{\nabla\,n}(\Delta\hat{\mathbf{u}}_{k-1}) + c_1\,\gamma_k\,\delta\Delta\hat{\mathbf{u}}_k^{\mathrm{T}}\,\mathbf{R}_{\mathrm{u}}(\Delta\hat{\mathbf{u}}_{k-1}) \tag{B.4}$$

where $\mathbf{R}_{\mathrm{u}}$ is the global displacement residual vector defined in (54) and $\mathbf{R}_{\mathrm{u}}(\Delta\hat{\mathbf{u}}_{k-1})$ is the residual at the previous iteration used for the computation of $\delta\Delta\hat{\mathbf{u}}_k$. The constant parameter c_1 for Newton type solver has the typical value 10^{-4} (see [50]).

Algorithm 3: Backtracking or steepest descent line search

`set` $\gamma_k = 1$

while (*.not. Wolfe*) **do**

  `update` $\gamma_k = \gamma_k\,\rho$

  `Wolfe` $\Pi_p^{\nabla\,n}(\Delta\hat{\mathbf{u}}_{k-1} + \gamma_k\,\delta\Delta\hat{\mathbf{u}}_k) < \Pi_p^{\nabla\,n}(\Delta\hat{\mathbf{u}}_{k-1}) + c_1\,\gamma_k\,\delta\Delta\hat{\mathbf{u}}_k^{\mathrm{T}}\,\mathbf{R}_{\mathrm{u}}(\Delta\hat{\mathbf{u}}_{k-1})$

end

The backtracking or steepest descent line search algorithm is shown in Algorithm 3. The idea is that the step length γ_k is reduced by a constant parameter $\rho \in [1/10, 1/2]$. Furthermore, a minimum value $\gamma_{k,min}$ should not be reached as suggested in [50]. An important remark must be done on the Dirichelet boundary condition of the displacement field. The minimization outlined in (B.4) must hold for all the active degrees of freedom, i.e., the degrees of freedom that contribute to the minimization of the total energy in the time step. Therefore, the constrained degrees of freedom must be excluded from the algorithm. Yet, in order to avoid a too large difference in the increment update of the active degrees of freedom and the constrained degrees of freedom a not too small threshold must be used for the step length. The choosen value is $\gamma_{k,min} = 1/2$.

Appendix C. Linear activation criterions

The use of von-Mises plasticity with linear isotropic hardening results in the yield vector $\mathbf{f}_{\mathrm{Y},e}$ to be a linear function of the plastic multiplier increment $\Delta\hat{\boldsymbol{\lambda}}_e$ as follows:

$$\begin{aligned}\mathbf{f}_{\mathrm{Y},e} &= \int_{\Omega_e} \left[\mathbf{N}_\lambda^{\mathrm{T}} \left(\sigma_{eq}^{tr} - 3G\,\Delta\lambda - \bar{\sigma}_{y0} - H\,\lambda\right) - c_p\,\mathbf{B}_\lambda^{\mathrm{T}}\,\boldsymbol{\nabla}\lambda\,\right] \mathrm{d}\Omega_e = \\ &= \underbrace{\int_{\Omega_e} \left[\mathbf{N}_\lambda^{\mathrm{T}} \left(\sigma_{eq}^{tr} - \bar{\sigma}_{y0} - H\,\lambda_n\right) - c_p\,\mathbf{B}_\lambda^{\mathrm{T}}\,\boldsymbol{\nabla}\lambda_n\,\right] \mathrm{d}\Omega_e}_{\mathbf{f}_{\mathrm{Y},e}^{tr}} + \\ &\quad \underbrace{-\left\{\int_{\Omega_e} \left[\left(3G + H\right)\mathbf{N}_\lambda^{\mathrm{T}}\,\mathbf{N}_\lambda + c_p\,\mathbf{B}_\lambda^{\mathrm{T}}\,\mathbf{B}_\lambda\,\right] \mathrm{d}\Omega_e\right\}}_{\mathbf{K}_{\lambda\lambda,e}} \Delta\hat{\boldsymbol{\lambda}}_e\end{aligned} \tag{C.1}$$

where the constant matrix $\mathbf{K}_{\lambda\lambda,e}$ has already been defined in (A.3c), while the element trial yield vector is defined as:

$$\mathbf{f}_{\mathrm{Y},e}^{tr} := \int_{\Omega_e} \left[\mathbf{N}_\lambda^{\mathrm{T}} \left(\sigma_{eq}^{tr} - \bar{\sigma}_{y0} - H\,\lambda_n\right) - c_p\,\mathbf{B}_\lambda^{\mathrm{T}}\,\boldsymbol{\nabla}\lambda_n\,\right] \mathrm{d}\Omega_e \tag{C.2}$$

On the other hand, the choices of a quadratic degradation function and the use of an AT1 dissipation functional for the phase field lead to the following definition of the phase-field activation vector $\mathbf{f}_{\mathrm{D},e}$:

$$\begin{aligned}\mathbf{f}_{\mathrm{D},e} &= \int_{\Omega_e} \left\{\mathbf{N}_{\mathrm{d}}^{\mathrm{T}} \left[\,2(1-d)\,\tilde{\psi}_0 - (f+1)\,\frac{3G_c}{8l_{0d}} + w'_\epsilon - \frac{\eta_f}{\Delta t}\,\Delta d\,\right] - \frac{3G_c l_{0d}}{4}\,\mathbf{B}_{\mathrm{d}}^{\mathrm{T}}\,\boldsymbol{\nabla} d\right\} \mathrm{d}\Omega_e = \\ &= \underbrace{\int_{\Omega_e} \left\{\mathbf{N}_{\mathrm{d}}^{\mathrm{T}} \left[2(1-d_n)\,\tilde{\psi}_0 - (f+1)\,\frac{3G_c}{8l_{0d}} + w'_\epsilon\right] - \frac{3G_c l_{0d}}{4}\,\mathbf{B}_{\mathrm{d}}^{\mathrm{T}}\,\boldsymbol{\nabla} d_n\right\} \mathrm{d}\Omega_e}_{\mathbf{f}_{\mathrm{D},e}^{tr}} - \\ &\quad \underbrace{-\left\{\int_{\Omega_e} \left\{\mathbf{N}_{\mathrm{d}}^{\mathrm{T}}\,\mathbf{N}_{\mathrm{d}} \left[\,2\,\tilde{\psi}_0 + \frac{\eta_f}{\Delta t}\right] + \frac{3G_c l_{0d}}{4}\,\mathbf{B}_{\mathrm{d}}^{\mathrm{T}}\,\mathbf{B}_{\mathrm{d}}\right\} \mathrm{d}\Omega_e\right\}}_{\mathbf{K}_{dd,e}} \Delta\hat{\mathbf{d}}_e\end{aligned}$$

where the trial elastoplastic activation vector $\mathbf{f}_{\mathrm{D},e}^{tr}$ and the the matrix $\mathbf{K}_{dd,e}$ have been defined:

$$\mathbf{f}_{\mathrm{D},e}^{tr} := \int_{\Omega_e} \left\{\mathbf{N}_{\mathrm{d}}^{\mathrm{T}} \left[2(1-d_n)\,\tilde{\psi}_0 - (f+1)\,\frac{3G_c}{8l_{0d}} + w'_\epsilon\right] - \frac{3G_c l_{0d}}{4}\,\mathbf{B}_{\mathrm{d}}^{\mathrm{T}}\,\boldsymbol{\nabla} d_n\right\} \mathrm{d}\Omega_e \tag{C.3a}$$

$$\mathbf{K}_{dd,e} := -\int_{\Omega_e} \left\{\mathbf{N}_{\mathrm{d}}^{\mathrm{T}}\,\mathbf{N}_{\mathrm{d}} \left[\,2\,\tilde{\psi}_0 + \frac{\eta_f}{\Delta t}\right] + \frac{3G_c l_{0d}}{4}\,\mathbf{B}_{\mathrm{d}}^{\mathrm{T}}\,\mathbf{B}_{\mathrm{d}}\right\} \mathrm{d}\Omega_e \tag{C.3b}$$

Finally, the yielding and fracture activation criterions (53b) and (53c) can be written as follows:

$$\Delta\hat{\lambda} \geq \mathbf{0} \quad , \quad (\mathbf{f}_{\mathrm{Y}}^{tr} + \mathbf{K}_{\lambda\lambda}\,\Delta\hat{\lambda}) \leq \mathbf{0} \quad , \quad \Delta\hat{\lambda}^{\mathrm{T}}\,(\mathbf{f}_{\mathrm{Y}}^{tr} + \mathbf{K}_{\lambda\lambda}\,\Delta\hat{\lambda}) = 0 \tag{C.4a}$$

$$\Delta\hat{\mathbf{d}} \geq \mathbf{0} \quad , \quad (\mathbf{f}_{\mathrm{D}}^{tr} + \mathbf{K}_{dd}\,\Delta\hat{\mathbf{d}}) \leq \mathbf{0} \quad , \quad \Delta\hat{\mathbf{d}}^{\mathrm{T}}\,(\mathbf{f}_{\mathrm{D}}^{tr} + \mathbf{K}_{dd}\,\Delta\hat{\mathbf{d}}) = 0 \tag{C.4b}$$

They correspond to the Karush-Kuhn-Tucker conditions associated to the constrained minimization of the total energy with respect to the plastic multiplier and the phase field. The specific choices adopted for the constitutive functionals make them two symmetric linear complementarity problems of the standard form:

$$\mathbf{x} \geq \mathbf{0} \quad , \quad (\mathbf{q} + \mathbf{Q} \cdot \mathbf{x}) \leq \mathbf{0} \quad , \quad \mathbf{x}^{\mathrm{T}}\,(\mathbf{q} + \mathbf{Q} \cdot \mathbf{x}) = 0$$

The solution of these variational inequalities is sought by means of a Projected Successive Over-Relaxation algorithm (PSOR) as introduced in [33]. It has been used for gradient plasticity [32] and in phase-field brittle fracture [34].

References

[1] G. A. Francfort, J. J. Marigo, Revisiting brittle fracture as an energy minimization problem, Journal of the Mechanics and Physics of Solids 46 (8) (1998) 1319–1342. doi:10.1016/S0022-5096(98)00034-9.

[2] B. Bourdin, G. A. Francfort, J. J. Marigo, Numerical experiments in revisited brittle fracture, Journal of the Mechanics and Physics of Solids 48 (2000) 797–826. doi:10.1016/S0022-5096(99)00028-9.

[3] R. Alessi, J. J. Marigo, S. Vidoli, Gradient damage models coupled with plasticity and nucleation of cohesive cracks, Archive for Rational Mechanics and Analysis 214 (2014) 575–615. doi:10.1007/s00205-014-0763-8.

[4] M. Ambati, T. Gerasimov, L. De Lorenzis, Phase-field modeling of ductile fracture, Computational Mechanics 46 (2015) 10171040. doi:10.1007/s00466-015-1151-4.

[5] F. P. Duda, A. Ciarbonetti, P. J. Sánchez, A. E. Huespe, A phase-field/gradient damage model for brittle fracture in elastic-plastic solids, International Journal of Plasticity 65 (2015) 269–296. doi:10.1016/j.ijplas.2014.09.005.

[6] J. Choo, W. C. Sun, Coupled phase-field and plasticity modeling of geological materials: From brittle fracture to ductile flow, Computer Methods in Applied Mechanics and Engineering 330 (2018) 1–32. doi:10.1016/j.cma.2017.10.009.

[7] C. Huang, X. Gao, Development of a phase field method for modeling brittle and ductile fracture, Computational Materials Science 169 (2019) 109089. doi:10.1016/j.commatsci.2019.109089.

[8] J. Fang, C. Wu, J. Li, Q. Liu, C. Wu, G. Sun, Q. Li, Phase field fracture in elasto-plastic solids: Variational formulation for multi-surface plasticity and effects of plastic yield surfaces and hardening, International Journal of Mechanical Sciences 156 (2019) 382–396. doi:10.1016/j.ijmecsci.2019.03.012.

[9] B. Yin, M. Kaliske, A ductile phase-field model based on degrading the fracture toughness: Theory and implementation at small strain, Computer Methods in Applied Mechanics and Engineering 366 (2020) 113068. doi:10.1016/j.cma.2020.113068.

[10] J. Ulloa, P. Rodríguez, E. Samaniego, On the modeling of dissipative mechanisms in a ductile softening bar, Journal of Mechanics of Materials and Structures 11 (4) (2016) 463–490. doi:10.2140/jomms.2016.11.463.

[11] P. Rodriguez, J. Ulloa, C. Samaniego, E. Samaniego, A variational approach to the phase field modeling of brittle and ductile fracture, International Journal of Mechanical Sciences 144 (2018) 502–517. doi:10.1016/j.ijmecsci.2018.05.009.

[12] S. S. Shishvan, S. Assadpour-asl, E. Martínez-Pañeda, A mechanism-based gradient damage model for metallic fracture, Engineering Fracture Mechanics 255 (2021) 107927. doi:10.1016/j.engfracmech.2021.107927.

[13] J. Wambacq, J. Ulloa, G. Lombaert, S. François, Interior-point methods for the phase-field approach to brittle and ductile fracture, Computer Methods in Applied Mechanics and Engineering 375 (2021) 113612. doi:10.1016/j.cma.2020.113612.

[14] M. Ambati, R. Kruse, L. De Lorenzis, A phase-field model for ductile fracture at finite strains and its experimental verification, Computational Mechanics 57 (01 2016). doi:10.1007/s00466-015-1225-3.

[15] M. J. Borden, T. J. Hughes, C. M. Landis, A. Anvari, I. J. Lee, A phase-field formulation for fracture in ductile materials: Finite deformation balance law derivation, plastic degradation, and stress triaxiality effects, Computer Methods in Applied Mechanics and Engineering 312 (2016) 130–166. doi:10.1016/j.cma.2016.09.005.

[16] B. Talamini, M. R. Tupek, A. J. Stershic, T. Hu, J. W. Foulk, J. T. Ostien, J. E. Dolbow, Attaining regularization length insensitivity in phase-field models of ductile failure, Computer Methods in Applied Mechanics and Engineering 384 (2021) 113936. doi:10.1016/j.cma.2021.113936.

[17] T. Hu, B. Talamini, A. J. Stershic, M. R. Tupek, J. E. Dolbow, A variational phase-field model for ductile fracture with coalescence dissipation, Computational Mechanics 68 (2021) 311–335. doi:10.1007/s00466-021-02033-1.

[18] J. Han, S. Matsubara, S. Moriguchi, M. Kaliske, K. Terada, Crack phase-field model equipped with plastic driving force and degrading fracture toughness for ductile fracture simulation, Computational Mechanics 69 (2022) 151–175. doi:10.1007/s00466-021-02087-1.

[19] C. Miehe, F. Aldakheel, S. Teichtmeister, Phase-field modeling of ductile fracture at finite strains: A robust variational-based numerical implementation of a gradient-extended theory by micromorphic regularization, International Journal for Numerical Methods in Engineering 111 (2017) 816–863. doi:10.1002/nme.5484.

[20] M. Dittmann, F. Aldakheel, J. Schulte, P. Wriggers, C. Hesch, Variational phase-field formulation of non-linear ductile fracture, Computer Methods in Applied Mechanics and Engineering 342 (2018) 71–94. doi:10.1016/j.cma.2018.07.029.

[21] C. Miehe, F. Aldakheel, A. Raina, Phase field modeling of ductile fracture at finite strains: A variational gradient-extended plasticity-damage theory, International Journal of Plasticity 84 (2016) 1–32. doi:10.1016/j.ijplas.2016.04.011.

[22] R. Alessi, M. Ambati, T. Gerasimov, S. Vidoli, L. De Lorenzis, Comparison of phase-field models of fracture coupled with plasticity, in: Computational Methods in Applied Sciences, Vol. 46, Springer Netherland, 2018, pp. 1–21. doi:10.1007/978-3-319-60885-3_1.

[23] B. D. Reddy, J. B. Martin, T. B. Griffin, Extremal paths and holonomic constitutive laws in elastoplasticity, Quarterly of Applied Mathematics 45 (3) (1987) 487–502. doi:10.1090/QAM/910456.

[24] M. Ortiz, J. B. Martin, Symmetry-preserving return mapping algorithms and incrementally extremal paths: A unification of concepts, International Journal for Numerical Methods in Engineering 28 (8) (1989) 1839–1853. doi:10.1002/NME.1620280810.

[25] J. C. Simo, T. Honein, Variational formulation, discrete conservation laws, and path-domain independent integrals for elasto-viscoplasticity, Journal of Applied Mechanics 57 (3) (1990) 488–497. doi:10.1115/1.2897050.

[26] C. Comi, A. Corigliano, G. Maier, Extremum properties of finite-step solutions in elastoplasticity with nonlinear mixed hardening, International Journal of Solids and Structures 27 (8) (1991) 965–981. doi:10.1016/0020-7683(91)90094-V.

[27] C. Comi, G. Maier, U. Perego, Generalized variable finite element modeling and extremum theorems in stepwise holonomic elastoplasticity with internal variables, Computer Methods in Applied Mechanics and Engineering 96 (2) (1992). doi:10.1016/0045-7825(92)90133-5.

[28] A. Corigliano, Numerical analysis of discretized elastoplastic systems using the generalized mid-point time integration, Engineering Computations 11 (5) (1994) 389–411. doi:10.1108/02644409410799353/FULL/XML.

[29] C. Comi, U. Perego, A unified approach for variationally consistent finite elements in elastoplasticity, Computer Methods in Applied Mechanics and Engineering 121 (1) (1995) 323–344. doi:10.1016/0045-7825(94)00703-P.

[30] R. Alessi, J.-J. Marigo, C. Maurini, S. Vidoli, Coupling damage and plasticity for a phase-field regularisation of brittle, cohesive and ductile fracture: one-dimensional examples, International Journal of Mechanical Sciences 149 (2018) 559–576. doi:10.1016/j.ijmecsci.2017.05.047.

[31] C. Samaniego, J. Ulloa, P. Rodríguez, G. Houzeaux, M. Vázquez, E. Samaniego, A phase-field model for ductile fracture with shear bands: A parallel implementation, International Journal of Mechanical Sciences 200 (2021) 106424. doi:10.1016/j.ijmecsci.2021.106424.

[32] C. Comi, U. Perego, A generalized variable formulation for gradient dependent softening plasticity, International Journal for Numerical Methods in Engineering 39 (1996) 3731–3755. doi:10.1002/(SICI)1097-0207(19961115)39:21<3731::AID-NME24>3.0.CO;2-Z.

[33] O. Mangasarian, Solution of Symmetric Linear Complementarity Problems by Iterative methods, Journal of Optimization Theory and Applications 22 (1977) 465485. doi:10.1007/BF01268170.

[34] A. Marengo, A. Patton, M. Negri, U. Perego, A. Reali, A rigorous and efficient explicit algorithm for irreversibility enforcement in phase-field finite element modeling of brittle crack propagation, Computer Methods in Applied Mechanics and Engineering 387 (2021) 114137. doi:10.1016/j.cma.2021.114137.

[35] W. M. Garrison, N. R. Moody, Ductile fracture, Journal of Physics and Chemistry of Solids 48 (11) (1987) 1035–1074. doi:10.1016/0022-3697(87)90118-1.

[36] E. Tanné, T. Li, B. Bourdin, J.-J. Marigo, C. Maurini, Crack nucleation in variational phase-field models of brittle fracture, Journal of the Mechanics and Physics of Solids 110 (2018) 80–99. arXiv:1203.1513, doi:10.1016/j.jmps.2017.09.006.

[37] A. Kumar, B. Bourdin, G. A. Francfort, O. Lopez-Pamies, Revisiting nucleation in the phase-Field approach to brittle fracture, Journal of the Mechanics and Physics of Solids 142 (2020) 104027. doi:10.1016/j.jmps.2020.104027.

[38] B. Halphen, N. Q. Son, On generalized standard materials. [sur les materiaux standards generalises.], J Mec 14 (1) (1975) 39–63.

[39] E. C. Aifantis, On the role of gradients in the localization of deformation and fracture, International Journal of Engineering Science 30 (10) (1992) 1279–1299. doi:10.1016/0020-7225(92)90141-3.

[40] S. Forest, Micromorphic Approach for Gradient Elasticity, Viscoplasticity, and Damage, Journal of Engineering Mechanics 135 (3) (2009) 117–131. doi:10.1061/(ASCE)0733-9399(2009)135:3(117).

[41] R. De Borst, H.-B. Mühlhaus, Gradient-dependent plasticity: Formulation and algorithmic aspects, International Journal for Numerical Methods in Engineering 35 (3) (1992) 521–539. doi:10.1002/NME.1620350307.

[42] C. Miehe, F. Aldakheel, S. Mauthe, Mixed variational principles and robust finite element implementations of gradient plasticity at small strains, International Journal for Numerical Methods in Engineering 94 (2013) 1037–1074. doi:10.1002/nme.4486.

[43] L. Ambrosio, V. Tortorelli, Approximation of functional depending on jumps by elliptic functional via t-convergence, Communications on Pure and Applied Mathematics 43 (8) (1990) 999–1036. doi:10.1002/CPA.3160430805.

[44] C. Comi, U. Perego, Fracture energy based bi-dissipative damage model for concrete, International Journal of Solids and Structures 38 (36-37) (2001). doi:10.1016/S0020-7683(01)00066-X.

[45] H. Amor, J. J. Marigo, C. Maurini, Regularized formulation of the variational brittle fracture with unilateral contact: Numerical experiments, Journal of the Mechanics and Physics of Solids 57 (2009) 1209–1229. doi:10.1016/j.jmps.2009.04.011.

[46] C. Miehe, M. Hofacker, F. Welschinger, A phase field model for rate-independent crack propagation: Robust algorithmic implementation based on operator splits, Computer Methods in Applied Mechanics and Engineering 199 (2010) 2765–2778. doi:10.1016/j.cma.2010.04.011.

[47] D. P. Flanagan, T. Belytschko, A uniform strain hexahedron and quadrilateral with orthogonal hourglass control, International Journal for Numerical Methods in Engineering 17 (5) (1981) 679–706. doi:10.1002/nme.1620170504.

[48] T. Gerasimov, L. De Lorenzis, On penalization in variational phase-field models of brittle fracture, Computer Methods in Applied Mechanics and Engineering 354 (2019) 990–1026. doi:10.1016/j.cma.2019.05.038.

[49] H. Li, M. Fu, J. Lu, H. Yang, Ductile fracture: Experiments and computations, International Journal of Plasticity 27 (2) (2011) 147–180. doi:10.1016/j.ijplas.2010.04.001.

[50] J. Nocedal, S. J. Wright, Numerical Optimization, 2nd Edition, Springer, New York, NY, USA, 2006.